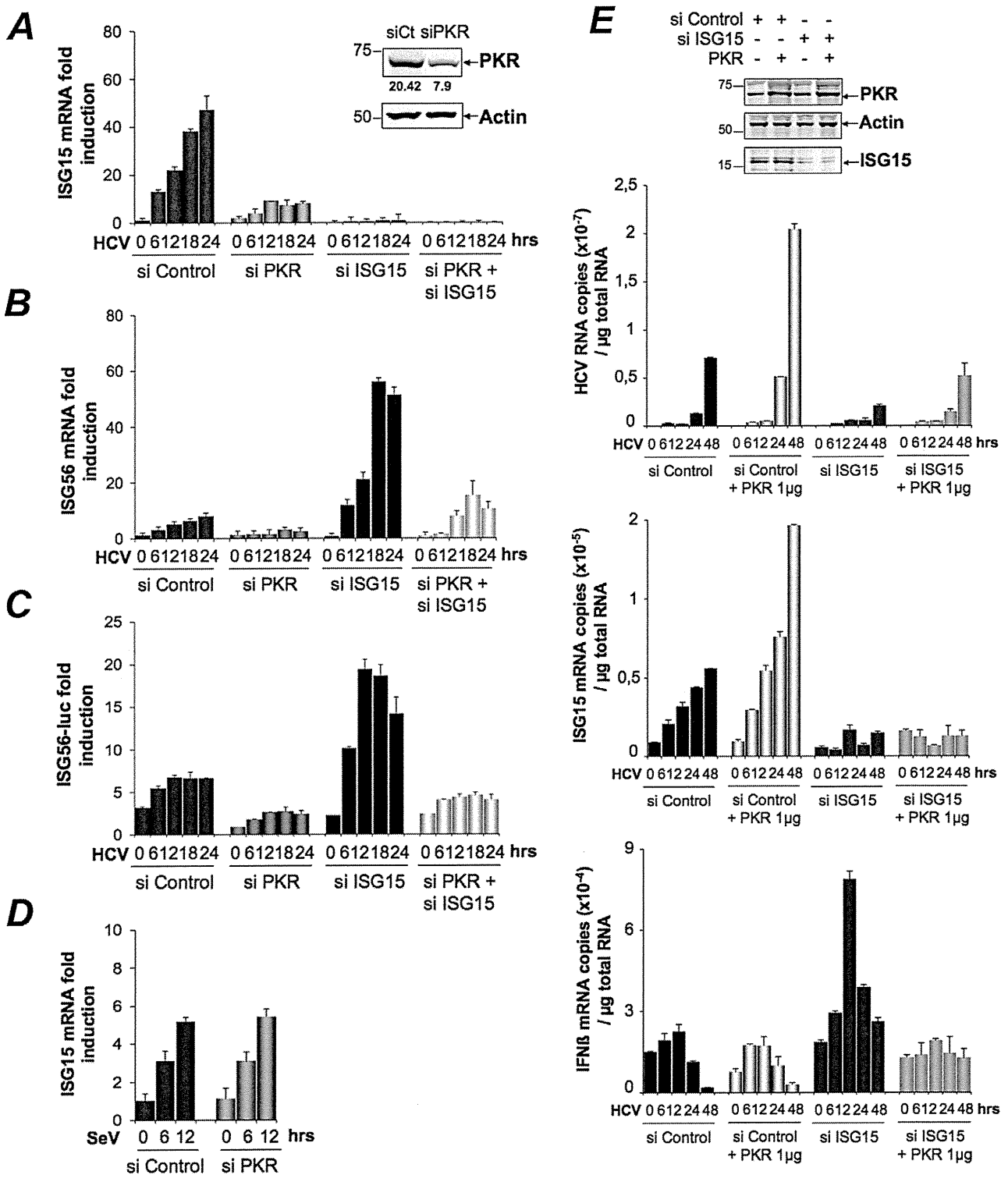

Figure 4. HCV triggers a PKR-dependent pathway early in infection to induce ISG15 and other genes. (**A–C**) The cDNAs reversed transcribed from the RNAs extracted from the Huh7.25.CD81 cells for the experiment described under Figure 3A were analysed by qPCR for the expression of ISG15 (**A**) and ISG56 (**B**). Expression levels of ISG15 and ISG56 RNA at the start of infection were respectively 1×10^5 and 1.18×10^5 copies. A novel set of Huh7.25.CD81 cells were transfected with siRNA Control, siRNA ISG15, siRNA PKR separately and together for 48 hrs. They were then transfected with the reporter plasmids ISG56-FLUC and pRL-TK-RLUC and infected with JFH1 (m.o.i = 0.2). At the times indicated, the effect of the different conditions of silencing on the reporter expression was analyzed after normalization performed as described under Figure 3C (**C**). Results are expressed as fold induction. Error bars represent the mean ±S.D for triplicates. (**D**) Huh7.25.CD81 cells were either transfected with 25 nM of siRNA Control or siPKR for 24 hrs and infected with SeV for the times indicated. Expression of endogenous ISG15 was determined by RTqPCR and expressed as fold induction. Error bars represent the mean ±S.D for triplicates. The expression levels of ISG15 RNA at the start of infection were respectively 4.91×10^4 copies (siControl) and 5.44×10^4 copies (siPKR). (**E**) Huh7.25.CD81 cells were either transfected with 25 nM of siRNA Control or

siISG15 and with 1 μg of a plasmid expressing PKR where indicated. After 48 hrs, the cells were infected with HCV (m.o.i = 6) for the times indicated. Expression of HCV, ISG15 and IFNβ RNA was determined by RTqPCR. Cell lysates prepared from cells treated in the same conditions but not infected were used to control expression of PKR and ISG15 by immunoblot.
doi:10.1371/journal.ppat.1002289.g004

use of the cell-penetrating ability of this peptide. Longer period of treatment with PRI were not investigated for practical reasons (see Materials and Methods). The results showed that PRI was significantly inhibiting the induction of ISG15 while it had no effect on that of IFNβ (**Figure 5F**). Altogether, these data demonstrate that HCV triggers induction of early ISGs through MAVS and TRAF3 by using PKR as an adapter protein.

PKR interacts both with MAVS and TRAF3 and binds HCV RNA ahead of RIG-I

The ability of HCV to control activation of the RIG-I/MAVS pathway after induction of ISG15 through a novel PKR/MAVS pathway suggests that PKR has the possibility to bind MAVS prior to RIG-I. To determine this, we established the kinetics of these interactions, after treating the Huh7.25.CD81 cells with siRNAs targeting ISG15 prior to HCV infection. This was necessary in view of the negative control of ISG15 on RIG-I. MAVS was immunoprecipitated from the cell extracts at different times post-infection and the presence of PKR and RIG-I was examined in the immunocomplexes, as well as that of TRAF3, used as marker of activation of the MAVS signaling pathway. As expected, only PKR was able to associate with MAVS and TRAF3 in the control cells (**Figure 6A**) whereas both PKR, RIG-I and TRAF3 were found in the immunocomplexes in the absence of ISG15 (**Figure 6B**). The PKR/MAVS association took place at 4 hrs post-infection in the control cells but was observed 2 hrs earlier in the ISG15-depleted cells. Whether ISG15 plays a role in the regulation of the PKR/MAVS association remains to be determined. However, the presence of TRAF3 in association with MAVS at 2 hrs post-infection in the control cells (**Figure 6A**) correlates with its association with PKR (**Figure 5C**) which indicates that the MAVS pathway can be activated through PKR as soon as 2 hrs post infection. In ISG15 knock-down cells, the RIG-I/MAVS association occurred later at 6 hrs post-infection with an increase in TRAF3 association at 9–12 hrs post infection. Altogether, these data revealed that HCV infection triggers an earlier interaction of MAVS with PKR than with RIG-I.

Finally, we asked whether PKR was able to associate with HCV RNA and how this association can be compared to that of RIG-I. PKR and RIG-I were immunoprecipitated at 2, 4 and 6 hrs post-infection and the presence of HCV RNA was analysed in the complexes. The results showed that PKR associates with HCV RNA with best efficiency at 2 hrs post-infection. Importantly, this association was strongly inhibited in presence of PRI, thus confirming the importance of PKR DRBD in the process. In contrast, the association of HCV RNA with RIG-I was detected only at 6 hrs post-infection. Interestingly, the association between RIG-I and HCV RNA was not affected by PRI, which rules out the possibility that the initial formation of a complex between PKR and HCV RNA was a pre-requisite for the subsequent binding of RIG-I to HCV RNA. Immunoprecipitation of PKR at 1, 2, 4 and 6 hrs post-infection, in presence of an inhibitor of ribonucleases also did not lead to detection of RIG-I in the complexes (**Figure S11**). Association of HCV RNA with eIF2α, used as negative control, was not significant, thus showing the specificity of the assay (**Figure 6C**). Whether a direct interaction of PKR with HCV RNA represents the initial event leading to the MAVS-dependent induction of early ISGs remains now to be characterized. Altogether, these data reveal an earlier mobilization of PKR than RIG-I in response to HCV infection which leads to activation of a MAVS-dependent signaling pathway.

Discussion

Hepatitis C virus can attenuate IFN induction at multiple levels in infected hepatocytes, such as through the NS3/4A-mediated MAVS cleavage [7,27] and by using the eIF2α kinase PKR to control IFN and ISG expression at the translational level [8,9]. Here, we have identified another process by which HCV controls IFN induction at the level of RIG-I ubiquitination through ISG15 and an ISGylation process. Importantly, we have shown that ISG15 is rapidly induced, among other ISGs, in response to HCV infection, through a novel signaling pathway that involves PKR, MAVS, TRAF3 and IRF3 but not RIG-I. In this pathway, PKR is not used for its kinase function but rather as an adapter protein with its dsRNA binding domain (DRBD) playing an essential role in this mechanism (**Figure 7**). By transcriptome analysis, we showed that HCV induces a number of ISGs in the HCV-permissive Huh7.25.CD81 cells and we confirmed the induction of two of these, ISG15 and ISG56, in other HCV-permissive cells, such as Huh7.5 and Huh7 cells. In addition, induction of ISG15 by HCV in a PKR-dependent manner was confirmed in human primary hepatocytes. The ability of HCV to trigger high expression levels of ISG15 and ISG56, as well as other ISGs, has previously been reported in models of HCV-infected chimpanzees [10,12,28] and in HCV-infected patients [14,15,16]. Induction of ISGs thus represents a general propriety of the response of the cells to HCV. In addition to this, natural variations in intra-hepatic levels of ISG15 *in vivo* may increase the susceptibility of some patients to HCV infection. The ability of HCV to control RIG-I activity through ISG15 is important to note in view of several reports which highlight the importance of a role for ISG15 in the maintenance of HCV in livers [15,16] or in the control of HCV replication in cell cultures [17,25]. Our data provide an explanation for the presence of ISGs at high expression levels in HCV-infected patients [14,15,16] and in models of HCV-infected chimpanzees [10,12,28] in the absence of, or with poor IFN expression.

The 15 Kda ISG15, or Interferon Stimulated Gene 15 [29], also known as ubiquitin cross reactive protein (UCRP) [30], can be conjugated (ISGylation) to more than 150 cellular protein targets [31] through the coordinated action of three E1, E2 and E3-conjugating enzymes, in a process similar but not identical to ubiquitination. While both ubiquitin and ISG15 can use the same E2 enzyme UbcH8, Ube1L functions as a specific E1 enzyme for ISG15, in spite of its 45% identity with Ube1, the E1 enzyme for ubiquitin [32]. The major E3 ligase for human ISG15 is HERC5 [33].

Interestingly, RIG-I was identified as a target for ISG15, among other IFN-induced proteins or proteins involved in IFN action [31]. However, its activity appears to be negatively controlled by ISG15 and the ISGylation process, either as shown previously after cotransfection with the ISG15 and the ISG15-conjugating enzymes [18] or as shown here, in a model of infection with HCV. Indeed, ISG15 is now emerging as playing a proviral role in case of HCV infection. Several reports now highlight the importance of a role for ISG15 in the control of HCV replication in cell cultures [17,25] as well as in the maintenance of HCV in livers and

Table 1. PKR-dependent up-regulated genes upon HCV infection.

SiPKR mock/siCt	Name	Access. N.	siCtMock	siCt HCV	siCtMock'	siPKRHCV	LOG2*
0,6	**ISG56**	NM_001548	15,0	885,8	10,2	7,6	-6,3
0,7	**ISG15**	NM_005101	593,6	26061,9	410,6	283,5	-6,0
0,7	**IFI 9-27/IFITM1**	NM_003641	27,8	817,7	15,1	10,1	-5,5
1,2	**IFI1-8U**	NM_006435	24,0	597,7	10,9	7,2	-5,3
1,1	Olfactory Receptor 9I1	NM_001005211	26,6	473,1	10,1	4,8	-5,2
1,6	IFI1-8U	XM_084845	17,7	365,4	9,3	6,5	-4,9
0,8	**OASp100**	NM_006187	46,4	909,9	40,0	33,5	-4,5
0,8	**IFI6-16**	NM_002038	834,5	10040,6	45,9	24,1	-4,5
0,6	**Ub2L6**	NM_004223	392,7	4078,9	281,2	128,7	-4,5
0,9	**OAS 1**	NM_016816	49,9	704,03	31,8	21,6	-4,4
0,9	**ISG12**	NM_005532	46,3	592,54	38,3	29,2	-4,1
0,8	**IFP 35**	NM_005533	36,3	369,7	26,6	16,9	-4,0
0,6	PARP-9	NM_031458	29,5	318,5	37,8	25,6	-4,0
0,5	GABA-B receptor 1	NM_006398	29,5	500,8	26,0	28,5	-4,0
0,7	**Lysp100B**	NM_003113	8,7	93	8,5	6,1	-3,9
0,8	PDIP1	NM_033405	27,4	146,6	28,0	12,8	-3,6
0,8	**PKR**	NM_002759	48,2	306,8	47,0	26,0	-3,5
1,6	**MT-IM**	NM_176870	49,0	1371,8	6,9	19,6	-3,3
0,7	**Phospholipid scramblase**	NM_021105	170	1137,2	189,9	153	-3,1
1,1	**RIG-I**	NM_014314	23,5	223,2	18,9	21,9	-3,0
0,6	**IFIT-5**	NM_012420	24,9	95,3	35,0	21,3	-2,7
1,3	RIG-I	NM_004585	7,4	42,5	6,3	6,0	-2,6
0,7	**STAT1 beta**	NM_139266	336,9	1401,5	300,3	210,3	-2,6
0,8	BRCA1 C-ter assoc. Prot	NM_001040444	12,3	45,1	8,1	5,1	-2,6
0,9	Cohesin Rec8 homolog	NM_005132	18,0	103	16,7	16,9	-2,5
0,5	C/EBPdelta	NM_005195	324,9	901,8	278,9	161,27	-2,3
0,7	ZNF532	NM_018181	32,8	146,5	25,5	23,8	-2,3
0,6	NNMT	NM_006169	52,8	143,8	50,26	28,9	-2,2
1	ISG1-8U	XM_084845	32,0	146,8	23,1	22,7	-2,2
1,1	HIF00	NM_153833	45,3	199,9	34,7	32,9	-2,2
0,8	**ISG20**	NM_002201	129,3	338,3	107,5	61,4	-2,2
1,1	PSMB10	NM_002801	16,2	75,1	14,5	15,0	-2,2
1,3	ZC3HAV1	NM_024625	8,3	26,0	6,9	4,9	-2,1
0,9	SOD2	NM_000636	348,5	1612,2	311	334,3	-2,1
0,7	PARP12	NM_022750	269,9	875,2	296,9	224,2	-2,1
0,7	NMI	NM_004688	32,1	136	37,4	37,0	-2,1
0,8	NEDD9	NM_006403	5,7	19,0	5,7	4,7	-2,0
1,1	**SAMHD1**	NM_015474	17,1	49,5	13,6	9,7	-2,0
0,7	AKT2	NM_001626	13,4	20,0	14,2	5,4	-2,0
0,5	ARG1	NM_000045	245,9	282,6	231,4	67,0	-2,0
0,8	BHLHB2	NM_003670	76,4	128,0	71,5	30,5	-2,0
0,8	LGALS3BP	NM_005567	22,0	72,0	16,1	13,6	-2,0
1,3	ZNF292	XM_048070	22,3	31,4	20,2	7,3	-2,0
1,1	STAT1	NM_007315	53,3	275,3	48,2	64,9	-1,9
0,7	TBA3_HUMAN	NM_006009	28,2	43,6	33,4	13,7	-1,9
0,5	TM4SF20	NM_024795	45,2	51,0	36,9	11,1	-1,9
1,4	ERAP2	NM_022350	9,8	19,2	8,8	4,6	-1,9
0,8	**USP18**	XM_001126794.1	215,1	979,2	201,8	245,9	-1,9
1	USP18	XM_001126794.1	129,6	617,0	127,3	165,5	-1,9

Table 1. Cont.

The Huh7.25.CD81 cells, seeded at 3.10^6 cells in 10-cm plates, were transfected after 24 hrs with 25 nM of siRNA Control or siRNA PKR using Fugene HD. 24 hrs post transfection, they were either mock-infected or infected for 2 hrs at 37°C with JFH1 (moi = 0.2) (three independent plates/sample). The medium was then removed and cells were incubated with complete DMEM for 12 hrs at 37°C. The cells were washed twice with TBS containing phosphatase and protease inhibitors, harvested by scraping, the cell pellets were centrifuged, the supernatants were removed and the pellets were frozen and stored at −80°C before being processed for micro-array.The list shows genes that were affected no more than twice by the depletion of PKR in the control cells (0.5< siPKR mock/siCt <1.6). The dependence of each of these genes in regards with PKR for their induction by HCV is expressed as log2 (ratio (siPKR HCV/siCt Mock)−(siCt HCV/siCt Mock) (indicated by log2*) with a cut-off of ≈2.0 fold.

doi:10.1371/journal.ppat.1002289.t001

pinpoint ISG15 as among the predictor genes of non-response to IFN therapy [14,15,16].

At present, we do not know at which level ISGylation regulates IFN induction in response to HCV infection. An HCV-mediated increase of ISG15 would favour preferential binding of ISG15 over that of ubiquitin to the E2 enzyme UbcH8 and hence enhance the spatio-temporal availability of UbcH8-ISG15 for HERC5 over that of UbcH8-ubiquitin for TRIM25. It may also lead to inhibition of TRIM25, through autoISGylation [21,34], which would decrease its ability to ubiquitinate RIG-I. We showed that overexpression of HERC5 together with Ube1L, UbcH8 and ISG15 was increasing the ability of ISG15 to inhibit IFN induction by HCV (**Figure 2B**). All three enzymes Ube1L, UbcH8 and HERC5 belong to the family of genes induced by IFN and it has been reported that ISGylation is optimum in a context of IFN treatment [18,35]. Therefore, it is tempting to speculate that elevated levels of ISG15 in some HCV-infected patients would bring the most favourable context for the virus when those patients are under IFN therapy. This would be in accord with the clinical data showing that HCV-induced high expression of ISG act as a negative predictive marker for response to IFN therapy.

It is doubtful that viruses with high IFN-inducing efficiency, such as Sendai virus may control RIG-I through ISG15 and PKR. However, viruses that avoid inducing IFN may have use of the PKR pathway. A good example might be that of Hepatitis B Virus (HBV) [36,37,38]. PKR expression was previously reported to be elevated in HCC liver from chronically HBV infected patients [39] and a relationship between PKR and IFN induction during HBV infection would be important to evaluate.

At present, we have established that HCV RNA interacts with PKR as soon as 2 hours post-infection. This interaction occurs prior the interaction of HCV RNA with RIG-I, which suggests that PKR may rapidly detect structures containing the incoming HCV RNA genome. Indeed, PKR has been reported to bind the dsRNA domains III and IV of HCV IRES [40] in addition to its ability to also bind 5′ triphosphorylated ss or dsRNA structures [41]. Whether PKR behaves as a pathogen recognition receptor for HCV RNA, like RIG-I, remains to be clarified. It is however clear that, in contrast to RIG-I, PKR acts here in favour of the pathogen rather than in favour of the host defense. We have established that the HCV RNA/PKR interaction depends on the first DRBD present at the N terminus of PKR and is independent on its kinase activity. The ability of PKR to serve as adapter in signaling pathways is not a total surprise since it has been previously shown to activate NF-κB through interaction of its C terminus with members of the TRAF family, such as TRAF5 and TRAF6 [42]. PKR contains also TRAF interacting motif in its N terminus [42] and an association between TRAF3 and PKR has been reported upon cotransfection in 293T cells [43]. Intriguingly, PKR was previously reported to participate in the induction of IFNβ, in association with MAVS, through activation of NF-κB or ATF-2 but not or partially IRF3; however these studies were not performed in the absence of RIG-I [44,45,46]. The mode of interaction between PKR, TRAF3 and MAVS, independently of RIG-I, and how it leads to a preferential induction of ISGs and not of IFNβ in response to HCV infection in contrast with the RIG-I/MAVS pathway remains to be determined. Based on our data, we propose now to divide the innate response to acute HCV infection into two phases: an early acute phase in which PKR is activated and a late acute phase that depends on RIG-I, the early phase controlling activation of the late phase. It is now essential to progress towards the generation of specific pharmaceutical inhibitors targeting PKR in order to abrogate the early acute phase to the benefit of the RIG-I-driven late phase. In a more general view, care should now be taken in the choice of compounds designed to be used as immune adjuvants, such as to be devoid of activation of the early acute PKR phase. This will ensure their efficiency as to activate properly the innate immune response through the late acute RIG-I phase.

Methods

Cell cultures and viruses

The culture of Huh7, Huh7.5, Huh7.25.CD81 cells, the preparation of Sendai virus stocks (≈2000 HAU/ml) and of HCV JFH1 stocks (≈6.10^4 FFU/mL and ≈6.10^6 FFU/mL) was as described [8,47]. Preparation and cultures of human primary hepatocytes was as described [48]. Of note, the ability of the Huh7.25.CD81 cells to induce IFN in response to SeV without prior IFN treatment (40-fold) was not observed in our previous study [8].The ability of Sendai virus to induce IFN is related to the presence of copyback DI (Defective Interfering) genomes [49]. The higher IFN inducing ability of the novel Sendai virus stock may have come from an important accumulation of these copyback DI genomes, during its growth in chicken eggs.

PKR inhibitors

The C16 compound [50] and the cell-permeable PRI peptide [51] were provided by Jacques Hugon. These drugs were applied (200 nM for C16 and 30 mM for PRI) one hour before the end of the 2 hr- incubation time with JFH1 and re-added to the medium after washing the cells with phosphate buffered saline (PBS). Note that PRI loses its effect very rapidly, probably through degradation in the cells, and requires to be added every hour to the cells until the end of treatment.

Expression vectors

TRIM25 was cloned from the IFN-treated Huh7.25CD81 cells (500 U/ml IFN-α2a; Cellsciences) after RT-PCR using the forward: 5′-ATGGCAGAGCTGTGCCCCCT-3′ and reverse 5′-CTACTTGGGGGAGCAGATGG-3′ primers. The pcDNA3.1(+) vector expressing 5′HA tagged-TRIM25 (provided by D. Garcin; University of Geneva, Switzerland) was used to generate the TRIM25 $P_{358}L$ construct by site-directed mutagenesis. The

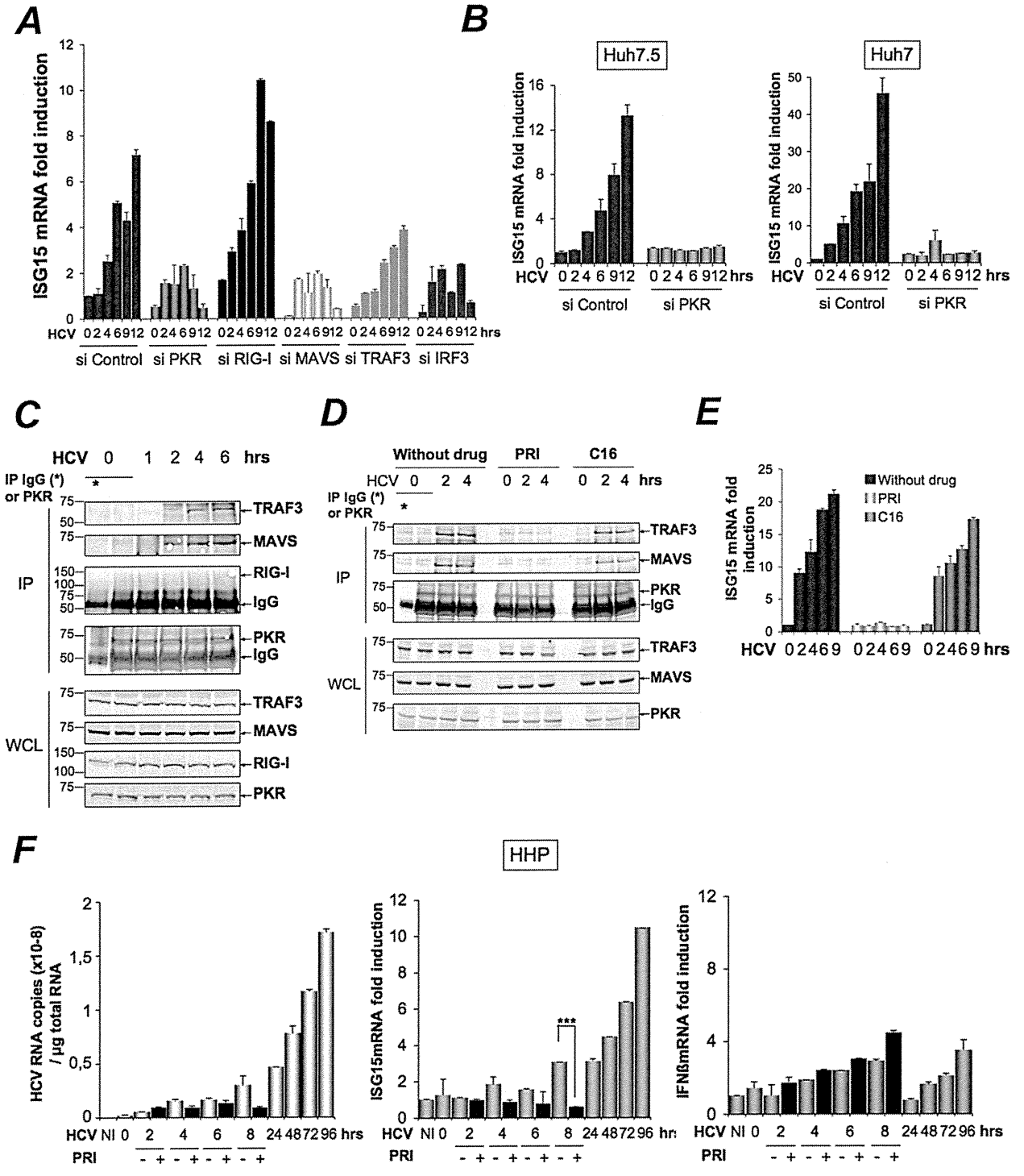

Figure 5. HCV-dependent induction of ISG15 involves PKR, MAVS and TRAF3 and not RIG-I. (**A–B**). **A**-The Huh7.25.CD81 cells were transfected with 50 nM Control siRNA and the different Smartpool siRNAs (50 nM siPKR; 10 nM siRIG-I; 5 nM siMAVS; 50 nM siTRAF3; 50 nM siIRF3) for 48 hrs and infected with JFH1 (m.o.i = 6). (**B**) Huh7.5 or Huh7 cells were transfected with siRNA Control or siPKR (50 nM) for 48 hrs and infected with JFH1 (m.o.i = 0.2 for Huh7.5 or 10 for Huh7). At the times indicated, expression of endogenous ISG15 was determined by RTqPCR and expressed as fold induction. Error bars represent the mean ±S.D for triplicates. The expression level of ISG15 RNA at the start of infection in the siControl cells was 9.97×10^4 copies (Huh7.25.CD81), 1.31×10^4 copies (Huh7.5) and 1.28×10^4 (Huh7). (**C–D**) Huh7.25.CD81 cells, in 100 cm^2 plates, were infected with JFH1 (m.o.i = 0.2) alone (**C**) or in presence of PRI or C16 (**D**). At the times indicated, cell extracts (3.5 mg) were processed for immunoprecipitation of PKR or for incubation with mouse IgG as a control of specificity (asterisk). The detection of the proteins in the complexes and in the whole cell extracts (WCE) was revealed by immunoblot using the Odyssey procedure. (**E**) The Huh7.25.CD81 cells were incubated with PRI or C16 and infected with JFH1 (m.o.i = 0.2) for the times indicated. Expression of endogenous ISG15 was determined as in A–B. The ISG15 RNA levels were 3.81×10^4 copies in the siControl cells. (**F**) Human primary hepatocytes (HHP) were infected with JFH1 (m.o.i = 6). One set of cells was incubated with 30 mM of the PRI inhibitor during 8 hours. At the times indicated, expression of HCV RNA, ISG15 and IFNβ was determined by RTqPCR. The expression levels of ISG15 and IFNβ RNA at the start of infection was 1.05×10^5 copies and $1,11\times10^4$ copies, respectively. Inhibition of induction of ISG15 by PRI at 8 hr post-infection was statistically significant (***; p = 0.0001).

doi:10.1371/journal.ppat.1002289.g005

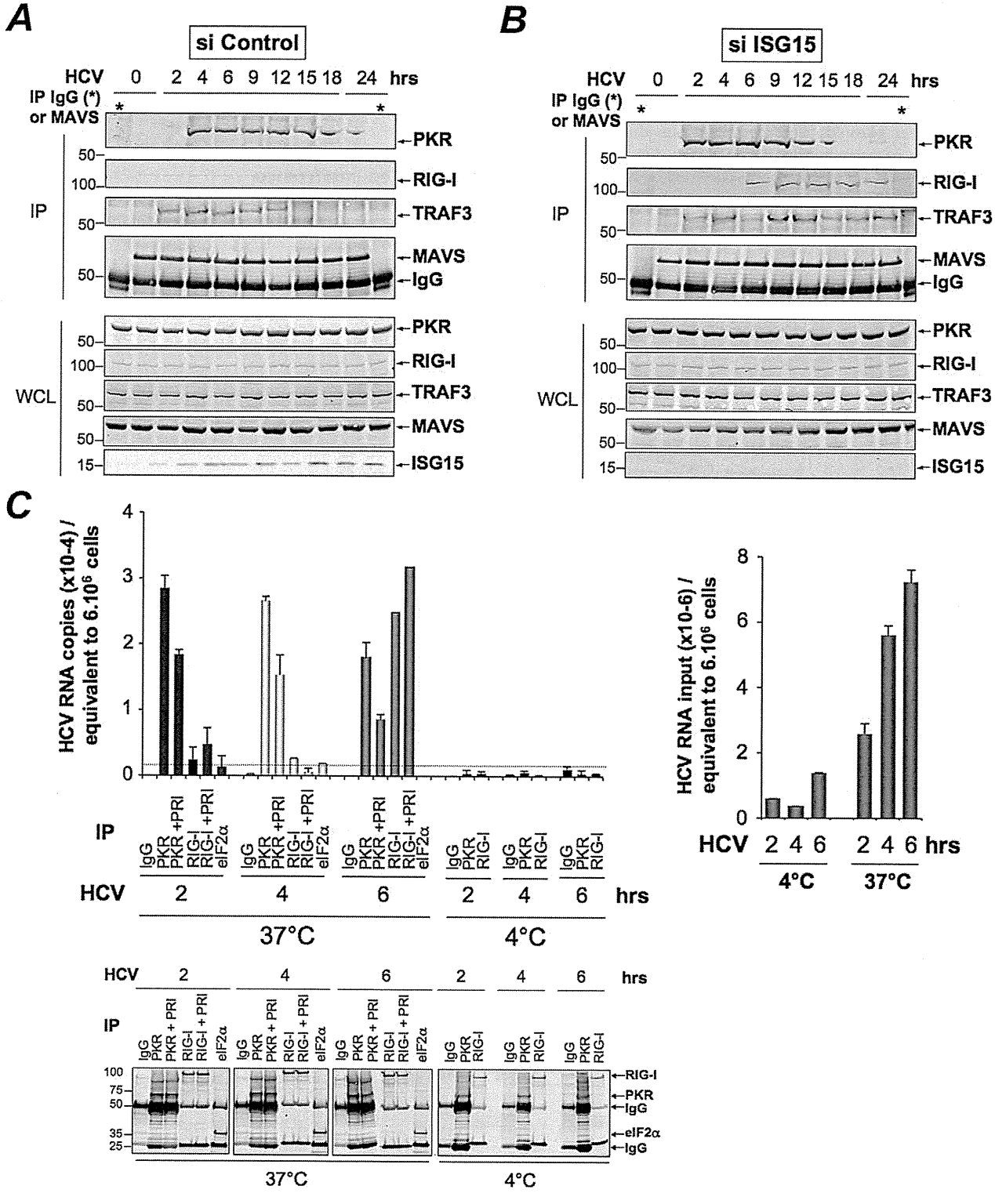

Figure 6. PKR both interacts with MAVS and TRAF3 and binds HCV RNA ahead of RIG-I. (**A–B**)- Huh7.25.CD81 cells were transfected with 25 nM of siRNA Control (**A**) or 25 nM of siRNA ISG15 (**B**) for 48 hrs and infected with JFH1 (m.o.i = 0.2). At the times indicated, cell extracts (4.5 mg) were incubated with anti-MAVS antibodies. In addition, cell extracts prepared at 0 hr post-infection were incubated with mouse IgG as a control of specificity (asterisk). The immunoprecipitated complexes were run on three different NuPAGE gels and blotted using Mab 71/10, anti-MAVS, anti-RIG-I or anti-TRAF3 antibodies. The expression level of each protein was controlled in the total cell extracts. (**C**)- Huh7.25.CD81 cells were incubated with JFH1 (m.o.i = 6) for 2 hrs at 37°C or at 4°C in the absence or presence of 30 μM of PRI. This drug was applied one hour before the end of the incubation time. After washing the cells twice with PBS, the cells were further incubated for 2, 4 or 6 hrs at 37°C or at 4°C in the absence or presence of PRI (added every hour). The cell extracts were processed for crosslinking of RNA to proteins before lysis, as described in Materials and Methods and different immunoprecipitations were performed with antibodies directed against PKR, RIG-I or eIF2α. After extensive washing, the presence of HCV RNA linked to the immunocomplexes was analysed by RTqPCR and the presence of the proteins was verified by Western blot. Measure of HCV RNA in

the cell extracts allowed to estimate its percentage of binding to PKR as 1.09%, 0.47% and 0.25% at 2, 4 and 6 hrs post-infection respectively, and its percentage of binding to RIG-I as 0.34% at 6 hrs post-infection.
doi:10.1371/journal.ppat.1002289.g006

IFNβ-firefly luciferase (pGL2-IFNβ) and pRL-TK Renilla-luciferase reporter plasmids were described previously [8]. The pGL3 luciferase reporter construct containing the −3 to −654 nucleotides of the ISG56 promoter was provided by N.Grandvaux [52]. The Myc-HIS-Ubiquitin construct was provided by R.Kopito (Stanford University, CA). ISG15 was cloned from IFN-treated Huh7 cells using the forward: 5′- GGATCCCATGGGCT-GGGACCTGACGGTG-3′ and reverse 5′-CTCGAGCTCC-GCCCGCCAGGCTCTGT-3′ primers and inserted into the pcDNA3.1(+)HA vector. The Ube1L, UbcH8 and HERC5 constructs were kindly provided by Jon M. Huibregtse [35]. The pcDNA1/AMP vector expressing PKR has been described previously [53].

RNA-mediated interference

The siRNAs directed against PKR, MAVS, RIG-I, TRAF3 and IRF3 which were used for the experiment described in figure 5A correspond to pools of siRNA (Smartpool) obtained from Dharmacon Research, Inc. (Lafayette, CO), as well as siRNAs directed against Ube1L used in Figure 2B. Control (scrambled) siRNA and siRNA directed against PKR or ISG15, used in all other experiments, were chemically synthesized by Dharmacon

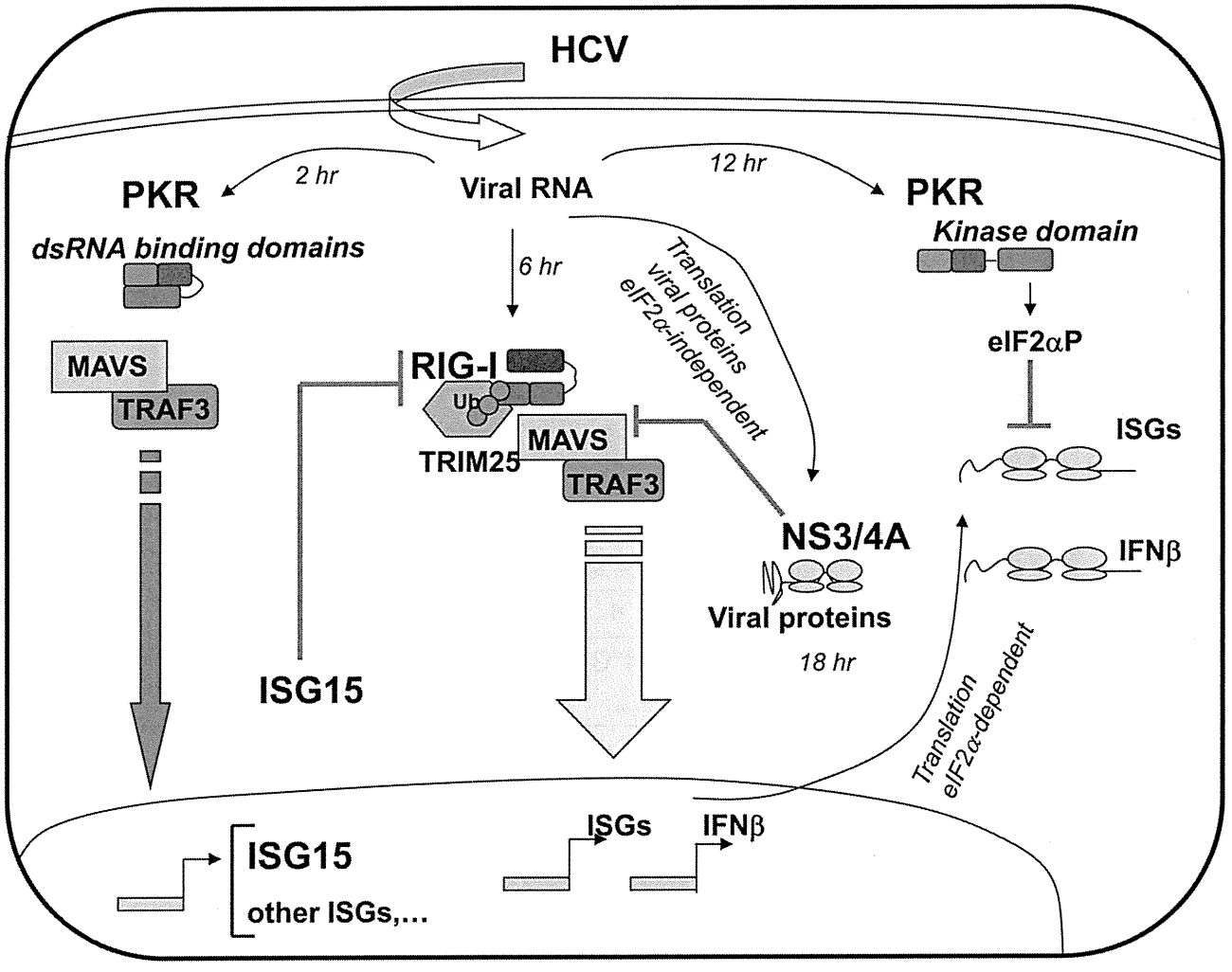

Figure 7. Multiple levels of control of IFN induction during HCV infection. Soon after infection, the HCV RNA is detected by the dsRNA binding domains (DRBD) of PKR ahead (2 hr) of its recognition by the RNA helicase RIG-I (6 hr). Recruitment of PKR by HCV triggers a signaling pathway that involves PKR as an adapter protein to recruit MAVS and TRAF3. This leads to a strong induction of the di-ubiquitine like protein ISG15 as well as other IRF3-dependent ISGs (Interferon-Stimulated Genes). ISG15 negatively controls the TRIM25-mediated ubiquitination (Ub) of RIG-I through an ISGylation process and thus interferes with the ability of RIG-I to recruit its downstream partners, including MAVS and TRAF3, and to induce IFNβ and ISGs. As the infection proceeds, HCV activates the eIF2α kinase function of PKR (12 hr). This leads to a transient (few hours) inhibition of general translation, including that of IFN [8] and ISGs [9] while the eIF2α-independent translation of the viral proteins proceeds unabated. At later times in the infection (18 hr), additional control of IFN induction occurs through cleavage of MAVS by the HCV NS3/4A protease, once the viral proteins have sufficiently accumulated in the cytosol [7,27].
doi:10.1371/journal.ppat.1002289.g007

(scrambled and PKR) and by EUROFINS MWG Operon (ISG15) (Text S1). The siRNAs (final concentration 25 nM or 50 nM) were transfected for 48 h using jetPRIME reagent according to the manufacturer's instructions (PolyPlus transfection TM) before transfection with other plasmids or before infection.

Antibodies

Mab to ISG15 (clone 2.1) was a kind gift of E.Borden [54]. Mab to PKR was produced from the murine 71/10 hybridoma (Agrobio; Fr) with kind permission of A.G.Hovanessian [55]. Other antibodies were as follows: anti-mouse IgG (Santa Cruz), anti-TRAF3 (Santa Cruz), pThr451-PKR (Alexis), MAVS (Alexis), anti-actin (Sigma), anti-pSer10-Histone H3 (Millipore), anti-HCV NS3 (Chemicon), anti-HCV core (Thermo scientific), anti-RIG-I (Alexis Biochemical Inc.), anti-TRIM25 (6105710; BD Bioscience), anti-IRF3 (Santa Cruz), anti-HA (12CA5; Roche) and anti-Myc (Santa Cruz).

Reporter assays

Huh7.25.CD81 cells (80,000 cells/well; 24-well plates) were transfected with 40 ng of pRL-TK Renilla-luciferase reporter (Promega) and 150 ng of either pGL2-IFNβ-Firefly luciferase reporter or pISG56-luciferase reporter and processed for dual-luciferase reporter assay as reported previously [8].

Real-time RT-PCR analysis

Total cellular RNA was extracted using the TRIZOL reagent (Invitrogen). HCV RNA was quantified by one-step RTqPCR. Reverse-transcription, amplification and real-time detection of PCR products were performed with 5 µl total RNA samples, using the SuperScript III Platinum one-step RTqPCR kit (Invitrogen) and an AbiPrism 7700 machine. For the sequence of the different primers, see Text S1. The results were normalized to the amount of cellular endogenous GAPDH RNA using the GAPDH control kit from EuroGentec. Copies number of HCV RNA may vary due to internal calibration and depending on the preparation of the viral stocks. All m.o.i were calculated using the titers expressed in FFU/ml. The IFNβ, ISG15, ISG56, Ube1L and GAPDH amplicons were quantified by a two-step RTqPCR assay as described [8].

Transcriptome analysis

Cellular RNA was extracted and purified from the cells using RNAeasy mini kit (QIAGEN K.K., Tokyo, Japan). Comprehensive DNA microarray analysis was performed with 3D-Gene Human Oligo chip25k with 2-color fluorescence method by New Frontiers Research Laboratories, Toray Industries Inc, Kamakura, Japan as previously described [56]. In brief, each sample was hybridized with 3D-Gene chip. Hybridization signals were scanned using Scan Array Express (PerkinElmer, Waltham, MA). The scanned image was analyzed using GenePix Pro (MDS Analytical Technologies, Sunnyvale, CA). All the analyzed data were scaled by global normalization.

Immunoprecipitation and immunoblot analysis

Cells were washed once with PBS and scraped into lysis buffer 1 (50 mM TRIS-HCl [pH 7.5], 140 mM NaCl, 5% glycerol, 1% CHAPS) that contained phosphatase and protease inhibitors (Complete, Roche Applied Science). The protein concentration was determined by the Bradford method. For immunoprecipitation, lysates were incubated at 4°C overnight with the primary antibodies as indicated and then in the presence of A/G-agarose beads (Santa Cruz Biotechnology) for 60 minutes. The beads were washed three times, and the precipitated proteins were extracted at 70°C using NuPAGE LDS sample buffer. Protein electrophoresis was performed on NuPAGE 4–12% Bis TRIS gels (Invitrogen). Proteins were transferred onto nitrocellulose membranes (Biorad), and probed with specific antibodies. Fluorescent immunoblot images were acquired and quantified by using an Odyssey scanner and the Odyssey 3.1 software (Li-Cor Biosciences) as described previously [8]. For detection of ISG15, cells were lysed in RIPA buffer (50 mM TRIS-HCl [pH 8.0]; 200 mM NaCl; 1% NP-40; 0.5% Sodium Deoxycholate; 0.05% SDS; 2 mM EDTA) and protein electrophoresis was performed on 4–20% polyacrylamide gels (PIERCE).

Nuclear/cytoplasmic extract

Pellets from cells washed in ice-cold phosphate-buffered saline (PBS) were lysed in ice-cold cytoplasmic buffer (10 mM TRIS [pH 8.0], 5 mM EDTA, 0.5 mM EGTA, 0.25% Triton X-100) containing phosphatase and protease inhibitors. The suspension was centrifuged for 30 seconds at 14,000 g and the supernatant (cytoplasmic fraction) was transferred into microcentrifuge tubes. The nuclear pellet was resuspended in Urea buffer (8 M Urea, 10 mM TRIS [pH 7,4], 1 mM EDTA, 1 mM dithiothreitol) containing phosphatase and protease inhibitors, homogenized by vortex and boiled for 10 minutes. The protein concentration was determined by the Bradford method.

Ubiquitination assay

Huh7.25.CD81 cells were transfected for 48 hrs with 5 µg of Myc-His-Ubiquitin expression plasmid using jetPRIME reagent. The cells were then washed in ice-cold PBS containing 20 mM N-ethylmaleimide (Sigma-Aldrich), harvested directly in Gua8 buffer (6 M guanidine-HCl, 300 mM NaCl, 50 mM Na_2HPO_4, 50 mM NaH_2PO_4 [pH 8.0]), briefly sonicated, and centrifuged at 14,000 g for 15 min at 4°C. 1/10th of the lysate was subjected to precipitation with 10% trichloroacetic acid for protein analysis in whole cell extracts. The rest of the lysate was incubated for 2 hrs with 20 µl (packed volume) of Talon resin Ni-affinity beads (Clontech) on a rotating wheel. Bound proteins were washed four times in Gua8 buffer, three times in Urea 6.3 buffer (8 M Urea, 10 mM TRIS, 0.1 M Na_2HPO_4, 20 mM Imidazole [pH 6.3]), and three times in cold PBS, after which they were eluted by boiling in NuPAGE LDS sample buffer. Electrophoresis was performed on 4–12% of acrylamide NuPAGE gels (Invitrogen).

Co-precipitation protein/HCV RNA

Huh7.25.CD81 cells were incubated for 10 min in their culture medium containing 1/10 volume (Vol) of a crosslinking solution (11% Formaldehyde, 0.1 M NaCl, 1 mM Na-EDTA-[pH 8], 0.5 mM Na-EGTA-[pH 8], 50 mM HEPES [pH 8]). The reaction was stopped by addition of a solution of 0.125 M glycine in PBS [pH 8] at room temperature (RT). The cells were washed three times in ice-cold PBS containing 1000 U/ml of RNAse inhibitor (Promega), scraped in PBS and dispatched into three sets containing ½ (set 1), ¼ (set 2) and ¼ (set 3) of the cell suspension. The three sets were centrifuged for 30 seconds at 14,000 g and 4°C and the cell pellets were lysed into lysis buffer 1 containing phosphatase/protease and RNAse inhibitors (Promega) for sets 1 and 2 or into TRIZOL reagent for set 3. Cell lysates from sets 1 and 2 were then incubated at 4°C, first overnight with the appropriate primary antibodies and for 60 minutes in the presence of A/G-agarose beads (Santa Cruz Biotechnology). After the incubation period, the beads were washed four times with buffer 1. Set 1 (HCV RNA bound to immunocomplexes) and set 3 (input HCV RNA) were submitted to TRIZOL treatment and HCV

RNA was quantified by one-step RTqPCR as described previously. The immunoprecipitated proteins from set 2 were extracted at 70°C using NuPAGE LDS sample buffer and analysed by immunoblot after electrophoresis on 4–12% of acrylamide NuPAGE gels (Invitrogen).

Supporting Information

Figure S1 Efficient induction of TRIM25 by IFN in the Huh7.25.CD81 cells. Huh7.25.CD81 cells, seeded at 8×10^4 cells in 24-well plates containing coverslips, were treated with 500 U/ml of IFNα for 24 hrs (IFN) or left untreated (Cont). Cells were fixed with 4% PFA and TRIM25 was detected using anti-TRIM25 antibodies (red). Nuclei are shown in blue after DAPI labelling. Microscope magnification was ×63.
(PDF)

Figure S2 HCV controls RIG-I ubiquitination through ISG15 in the Huh7 cells. Huh7 cells were transfected for 24 hrs with 25 nM of siRNA (Control or ISG15) and for another 24 hr with 5 μg of a His-Myc-Ubiquitin plasmid in absence or presence of 5 μg of a plasmid expressing HA-TRIM25. The cells were infected with JFH1 (m.o.i = 0.2). At the times indicated, cell extracts were processed for analysis of RIG-I ubiquitination and the expression of the different proteins in the total cell extracts. Efficiency of infection by JFH1 in the Huh7 cells was 2 log less than in the Huh7.25.CD81 cells.
(PDF)

Figure S3 Expression of ISG15 and ISG15 conjugating enzymes inhibit IFN induction in response to SeV. Huh7.25.CD81 cells were transfected with a plasmid expressing HA-ISG15 alone or in the presence of plasmids expressing the ISG15 conjugating enzymes Ube1L (E1), UbcH8 (E2) and HERC5 (E3). The cells were then infected with JFH1 (m.o.i = 6) for the times indicated. Stimulation of endogenous IFNβ RNA expression was determined by RTqPCR and expressed as fold induction. The degree of statistical significance is indicated by stars after calculation of the p-values (from left to right: 0.0124 and 0.0058).
(PDF)

Figure S4 Control of efficiency of siRNA Ube1L in the Huh7.25.CD81 cells. The Huh7.25.CD81 cells were transfected with 50 nM of siRNA directed against Ube1L for 48 hours and infected with HCV. RNA was prepared from the cells at different times post infection as indicated and expression levels of Ube1L was determined by RTqPCR.
(PDF)

Figure S5 Modulation of PKR activation by ISG15. Huh7.25.CD81 cells, in 100 cm^2 plates, were transfected with siRNA Control or siRNA ISG15 or transfected with a plasmid expressing HA-ISG15 for 48 hrs and infected with JFH1 (m.o.i = 6). At the indicated times post-infection, cell extracts (2.2 mg) were processed for immunoprecipitation of PKR. The immunoprecipitated complexes were run on two different NuPAGE gels and blotted using Mab 71/10 or anti-phosphorylated PKR antibodies (PKR-P). The presence of PKR and PKR-P was revealed using the Odyssey procedure. The bands corresponding to total PKR and phosphorylated PKR were quantified using the Odyssey software and expressed as the ratio PKR-P/PKR in the absence (siISG15) and in the presence of ISG15 in the control cells (Control) or after transfection of the ISG15 expressing plasmid (HA-ISG15).
(PDF)

Figure S6 Induction of ISG56 by Sendai virus in the Huh7.25.CD81 cells does not depend on PKR. Huh7.25.CD81 cells were either transfected with 25 nM of siRNA Control or 25 nM siPKR for 24 hrs and infected with SeV for the times indicated. The effect of PKR silencing on the stimulation of expression of endogenous ISG56 was determined by RTqPCR and expressed as fold induction. Error bars represent the mean ±S.D for triplicates. The expression levels of ISG56 RNA at the start of infection were respectively 1.15×10^5 copies (siControl) and 1.16×10^5 copies (siPKR).
(PDF)

Figure S7 Control of the efficiency of siRNA treatment in the Huh7.25.CD81 cells. The Huh7.25.CD81 cells were transfected for 48 hrs with 50 nM Control siRNA or with the different Smartpool siRNAs as shown (50 nM siPKR; 10 nM siRIG-I; 50 nM siIRF3; 50 nM siTRAF3; 5 nM siMAVS). Total cell extracts were prepared and the expression level of each protein, as well as that of actin used as control, was revealed by immunoblot and Odyssey procedure after a run on NuPAGE gels. Under each lane, the numbers represent the quantification of the different protein bands performed using the Odyssey software.
(TIF)

Figure S8 HCV triggers nuclear translocation of IRF3 early after infection in the Huh7.25.CD81 cells. Huh7.25.CD81 cells, seeded at 10^5 cells in 24-well plates containing coverslips, were infected for different times (0, 4 and 6 hours) at 37°C with JFH1 (moi = 6) or with SeV (40 HAU/ml) in the absence or in the presence of 10 ng/ml Leptomycine B (LB; Sigma), which was used here as a convenient mean to enhance the nuclear detection of IRF3 since it can interfere with nuclear export [57]. Cells were fixed with 4% PFA and IRF3 was detected using anti-IRF3 antibodies (red). Nuclei are shown in blue after DAPI labelling. The arrows show the presence of IRF3 in the nucleus. Microscope magnification was ×63.
(PDF)

Figure S9 Induction of ISG56 by HCV in the Huh7.5 and Huh7 cells depends on PKR. Huh7.5 or Huh7 cells were transfected with siRNA Control or siPKR (50 nM) for 48 hrs and infected with JFH1 (m.o.i = 0.2 for Huh7.5 or 10 for Huh7). At the times indicated, expression of endogenous ISG56 was determined by RTqPCR and expressed as fold induction. Error bars represent the mean ±S.D for triplicates. The expression levels of ISG56 RNA at the start of infection in the siControl cells was 1.37×10^4 copies (Huh7.5 cells) and 1.28×10^4 copies (Huh7 cells).
(PDF)

Figure S10 Induction of ISG56 by HCV is specifically inhibed by the PKR inhibitor PRI. The Huh7.25.CD81 cells were incubated with PRI or C16 and infected with JFH1 (m.o.i = 0.2) for the times indicated. RTqPCR analysis of endogenous ISG56 was determined by RTqPCR and expressed as fold induction. The expression levels of ISG56 RNA at the start of infection in the control cells was 1.97×10^4 copies.
(TIF)

Figure S11 The RNAse inhibitor RNAsin does not favour the formation of a RIG-I/PKR complex upon HCV infection. Two sets of Huh7.25.CD81 cells were plated into 100 cm^2 plates and infected with JFH1. At the times indicated, cell extracts (3.5 mg) from the two sets were processed similarly for immunoprecipitation of PKR or for incubation with mouse IgG as a control of specificity (asterisk), except that care was taken to add the RNAse inhibitor RNAsin (1000 U/ml) at all steps for the second set (+RNAsin). Detection of RIG-I, MAVS, and PKR in

the complexes and in the whole cell extracts (WCE) was revealed by immunoblot using the Odyssey procedure. Detection of Actin in WCE served as loading control.
(PDF)

Table S1 Transcriptome analysis of PKR-dependent downpregulated gene upon 12 hrs of HCV infection. Preparation of samples was as described under Table 1. The list shows genes that were affected no more than twice by the depletion of PKR in the control cells (0.5< siPKR mock/siCt <1.6). The dependence of each of these genes in regards with PKR for their inhibition by HCV is expressed as log2 (ratio (siPKR HCV/siCt Mock)−(siCt HCV/siCt Mock) (indicated by log2*) with a cut-off of ≈2.0 fold.
(DOC)

Text S1 Supplementary methods.
(DOC)

Acknowledgments

We thank Michael Gale Jr, Pierre-Olivier Vidalain and Christine Neuveut for critical reviews of the manuscript. We thank Adrien Six, Eric Batsche and Agata Budkowska for discussions. We thank Ernest Borden for the gift of anti-ISG15 antibodies, Jon Huibregste for the gift of plasmids expressing ISG15 conjugating enzymes, Dominique Garcin for providing the Sendai virus, Claire Gondeau and Martine Daujat for their help in the preparation and infection of human primary hepatocytes with JFH1.

Author Contributions

Conceived and designed the experiments: NA TW EFM. Performed the experiments: NA SD DA MF FS-O. Analyzed the data: NA TW EFM. Contributed reagents/materials/analysis tools: JH DA MF FS-O TW. Wrote the paper: NA EFM.

References

1. Gack MU, Shin YC, Joo CH, Urano T, Liang C, et al. (2007) TRIM25 RING-finger E3 ubiquitin ligase is essential for RIG-I-mediated antiviral activity. Nature 446: 916–920.
2. Gack MU, Kirchhofer A, Shin YC, Inn KS, Liang C, et al. (2008) Roles of RIG-I N-terminal tandem CARD and splice variant in TRIM25-mediated antiviral signal transduction. Proc Natl Acad Sci U S A 105: 16743–16748.
3. Yoneyama M, Fujita T (2009) RNA recognition and signal transduction by RIG-I-like receptors. Immunol Rev 227: 54–65.
4. Binder M, Kochs G, Bartenschlager R, Lohmann V (2007) Hepatitis C virus escape from the interferon regulatory factor 3 pathway by a passive and active evasion strategy. Hepatology 46: 1365–1374.
5. Saito T, Owen DM, Jiang F, Marcotrigiano J, Gale M, Jr. (2008) Innate immunity induced by composition-dependent RIG-I recognition of hepatitis C virus RNA. Nature 454: 523–527.
6. Sumpter R, Jr., Loo YM, Foy E, Li K, Yoneyama M, et al. (2005) Regulating intracellular antiviral defense and permissiveness to hepatitis C virus RNA replication through a cellular RNA helicase, RIG-I. J Virol 79: 2689–2699.
7. Meylan E, Curran J, Hofmann K, Moradpour D, Binder M, et al. (2005) Cardif is an adaptor protein in the RIG-I antiviral pathway and is targeted by hepatitis C virus. Nature 437: 1167–1172.
8. Arnaud N, Dabo S, Maillard P, Budkowska A, Kalliampakou KI, et al. (2010) Hepatitis C virus controls interferon production through PKR activation. PLoS One 5: e10575.
9. Garaigorta U, Chisari FV (2009) Hepatitis C virus blocks interferon effector function by inducing protein kinase R phosphorylation. Cell Host Microbe 6: 513–522.
10. Mihm S, Frese M, Meier V, Wietzke-Braun P, Scharf JG, et al. (2004) Interferon type I gene expression in chronic hepatitis C. Lab Invest 84: 1148–1159.
11. Sarasin-Filipowicz M, Oakeley EJ, Duong FH, Christen V, Terracciano L, et al. (2008) Interferon signaling and treatment outcome in chronic hepatitis C. Proc Natl Acad Sci U S A 105: 7034–7039.
12. Bigger CB, Guerra B, Brasky KM, Hubbard G, Beard MR, et al. (2004) Intrahepatic gene expression during chronic hepatitis C virus infection in chimpanzees. J Virol 78: 13779–13792.
13. Takahashi K, Asabe S, Wieland S, Garaigorta U, Gastaminza P, et al. (2010) Plasmacytoid dendritic cells sense hepatitis C virus-infected cells, produce interferon, and inhibit infection. Proc Natl Acad Sci U S A 107: 7431–7436.
14. Askarieh G, Alsio A, Pugnale P, Negro F, Ferrari C, et al. (2010) Systemic and intrahepatic interferon-gamma-inducible protein 10 kDa predicts the first-phase decline in hepatitis C virus RNA and overall viral response to therapy in chronic hepatitis C. Hepatology 51: 1523–1530.
15. Asselah T, Bieche I, Narguet S, Sabbagh A, Laurendeau I, et al. (2008) Liver gene expression signature to predict response to pegylated interferon plus ribavirin combination therapy in patients with chronic hepatitis C. Gut 57: 516–524.
16. Chen L, Borozan I, Feld J, Sun J, Tannis LL, et al. (2005) Hepatic gene expression discriminates responders and nonresponders in treatment of chronic hepatitis C viral infection. Gastroenterology 128: 1437–1444.
17. Chen L, Sun J, Meng L, Heathcote J, Edwards A, et al. (2010) ISG15, a ubiquitin-like interferon stimulated gene, promotes Hepatitis C Virus production in vitro: Implications for chronic infection and response to treatment. J Gen Virol 91: 382–388.
18. Kim MJ, Hwang SY, Imaizumi T, Yoo JY (2008) Negative feedback regulation of RIG-I-mediated antiviral signaling by interferon-induced ISG15 conjugation. J Virol 82: 1474–1483.
19. Akazawa D, Date T, Morikawa K, Murayama A, Miyamoto M, et al. (2007) CD81 expression is important for the permissiveness of Huh7 cell clones for heterogeneous hepatitis C virus infection. J Virol 81: 5036–5045.
20. Nisole S, Stoye JP, Saib A (2005) TRIM family proteins: retroviral restriction and antiviral defence. Nat Rev Microbiol 3: 799–808.
21. Zou W, Wang J, Zhang DE (2007) Negative regulation of ISG15 E3 ligase EFP through its autoISGylation. Biochem Biophys Res Commun 354: 321–327.
22. Jeon YJ, Yoo HM, Chung CH (2010) ISG15 and immune diseases. Biochim Biophys Acta 1802: 485–496.
23. Kim KI, Yan M, Malakhova O, Luo JK, Shen MF, et al. (2006) Ube1L and protein ISGylation are not essential for alpha/beta interferon signaling. Mol Cell Biol 26: 472–479.
24. Chen WH, Basu S, Bhattacharjee AK, Cross AS (2010) Enhanced antibody responses to a detoxified lipopolysaccharide-group B meningococcal outer membrane protein vaccine are due to synergistic engagement of Toll-like receptors. Innate Immun 16: 322–332.
25. Broering R, Zhang X, Kottilil S, Trippler M, Jiang M, et al. (2010) The interferon stimulated gene 15 functions as a proviral factor for the hepatitis C virus and as a regulator of the IFN response. Gut 59: 1111–1119.
26. Elco CP, Guenther JM, Williams BRG, Sen GC (2005) Analysis of genes induced by Sendai virus infection of mutant cell lines reveals essential roles of interferon regulatory factor 3, NF-kappaB, and interferon but not toll-like receptor 3. J Virol 79: 3920–3929.
27. Loo YM, Owen DM, Li K, Erickson AK, Johnson CL, et al. (2006) Viral and therapeutic control of IFN-beta promoter stimulator 1 during hepatitis C virus infection. Proc Natl Acad Sci U S A 103: 6001–6006.
28. Bigger CB, Brasky KM, Lanford RE (2001) DNA microarray analysis of chimpanzee liver during acute resolving hepatitis C virus infection. J Virol 75: 7059–7066.
29. Farell PJ, Broeze RJ, Lengyel P (1979) Accumulation of an mRNA and protein in interferon-treated Ehrlich ascites tumour cells. Nature (London) 279: 523–524.
30. Haas AL, Ahrens P, Bright PM, Ankel H (1987) Interferon induces a 15-kilodalton protein exhibiting marked homology to ubiquitin. J Biol Chem 262: 11315–11323.
31. Zhao C, Denison C, Huibregtse JM, Gygi S, Krug RM (2005) Human ISG15 conjugation targets both IFN-induced and constitutively expressed proteins functioning in diverse cellular pathways. Proc Natl Acad Sci U S A 102: 10200–10205.
32. Yuan W, Krug RM (2001) Influenza B virus NS1 protein inhibits conjugation of the interferon (IFN)-induced ubiquitin-like ISG15 protein. Embo J 20: 362–371.
33. Wong JJ, Pung YF, Sze NS, Chin KC (2006) HERC5 is an IFN-induced HECT-type E3 protein ligase that mediates type I IFN-induced ISGylation of protein targets. Proc Natl Acad Sci U S A 103: 10735–10740.
34. Zou W, Zhang DE (2006) The interferon-inducible ubiquitin-protein isopeptide ligase (E3) EFP also functions as an ISG15 E3 ligase. J Biol Chem 281: 3989–3994.
35. Durfee LA, Lyon N, Seo K, Huibregtse JM (2010) The ISG15 conjugation system broadly targets newly synthesized proteins: implications for the antiviral function of ISG15. Mol Cell 38: 722–732.
36. Wieland SF, Chisari FV (2005) Stealth and cunning: hepatitis B and hepatitis C viruses. J Virol 79: 9369–9380.
37. Jiang J, Tang H (2010) Mechanism of inhibiting type I interferon induction by hepatitis B virus×protein. Prein Cell 1: 1106–1117.
38. Wei C, Ni C, Song T, Liu Y, Yang X, et al. (2010) The hepatitis B virus×protein disrupts innate immunity by downregulating mitochondrial antiviral signaling protein. J Immunol 185: 1158–1168.
39. Chen GG, Lai PB, Ho RL, Chan PK, Xu H, et al. (2004) Reduction of double-stranded RNA-activated protein kinase in hepatocellular carcinoma associated with hepatitis B virus. J Med Virol 73: 187–194.

40. Shimoike T, McKenna SA, Lindhout DA, Puglisi JD (2009) Translational insensitivity to potent activation of PKR by HCV IRES RNA. Antiviral Res 83: 228–237.
41. Nallagatla SR, Hwang J, Toroney R, Zheng X, Cameron CE, et al. (2007) 5′-triphosphate-dependent activation of PKR by RNAs with short stem-loops. Science 318: 1455–1458.
42. Gil J, Garcia MA, Gomez-Puertas P, Guerra S, Rullas J, et al. (2004) TRAF family proteins link PKR with NF-kappa B activation. Mol Cell Biol 24: 4502–4512.
43. Oganesyan G, Saha SK, Guo B, He JQ, Shahangian A, et al. (2006) Critical role of TRAF3 in the Toll-like receptor-dependent and -independent antiviral response. Nature 439: 208–211.
44. Zhang P, Samuel CE (2008) Induction of protein kinase PKR-dependent activation of interferon regulatory factor 3 by vaccinia virus occurs through adapter IPS-1 signaling. J Biol Chem 283: 34580–34587.
45. McAllister CS, Samuel CE (2009) The RNA-activated protein kinase enhances the induction of interferon-beta and apoptosis mediated by cytoplasmic RNA sensors. J Biol Chem 284: 1644–1651.
46. McAllister CS, Toth AM, Zhang P, Devaux P, Cattaneo R, et al. (2010) Mechanisms of protein kinase PKR-mediated amplification of beta interferon induction by C protein-deficient measles virus. J Virol 84: 380–386.
47. Strahle L, Marq JB, Brini A, Hausmann S, Kolakofsky D, et al. (2007) Activation of the beta interferon promoter by unnatural Sendai virus infection requires RIG-I and is inhibited by viral C proteins. J Virol 81: 12227–12237.
48. Biron-Andreani C, Raulet E, Pichard-Garcia L, Maurel P (2010) Use of human hepatocytes to investigate blood coagulation factor. Methods Mol Biol 640: 431–445.
49. Strahle L, Garcin D, Kolakofsky D (2006) Sendai virus defective-interfering genomes and the activation of interferon-beta. Virology 351: 101–111.
50. Jammi NV, Whitby LR, Beal PA (2003) Small molecule inhibitors of the RNA-dependent protein kinase. Biochem Biophys Res Commun 308: 50–57.
51. Nekhai S, Bottaro DP, Woldehawariat G, Spellerberg A, Petryshyn R (2000) A cell-permeable peptide inhibits activation of PKR and enhances cell proliferation. Peptides 21: 1449–1456.
52. Grandvaux N, Servant MJ, tenOever B, Sen GC, Balachandran S, et al. (2002) Transcriptional profiling of interferon regulatory factor 3 target genes: direct involvement in the regulation of interferon-stimulated genes. J Virol 76: 5532–5539.
53. Bonnet MC, Daurat C, Ottone C, Meurs EF (2006) The N-terminus of PKR is responsible for the activation of the NF-kappaB signaling pathway by interacting with the IKK complex. Cell Signal 18: 1865–1875.
54. Malakhov MP, Kim KI, Malakhova OA, Jacobs BS, Borden EC, et al. (2003) High-throughput immunoblotting. Ubiquitiin-like protein ISG15 modifies key regulators of signal transduction. J Biol Chem 278: 16608–16613.
55. Laurent AG, Krust B, Galabru J, Svab J, Hovanessian AG (1985) Monoclonal antibodies to interferon induced 68,000 Mr protein and their use for the detection of double-stranded RNA dependent protein kinase in human cells. Proc Natl Acad SciUSA 82: 4341–4345.
56. Iwano S, Ichikawa M, Takizawa S, Hashimoto H, Miyamoto Y (2010) Identification of AhR-regulated genes involved in PAH-induced immunotoxicity using a highly-sensitive DNA chip, 3D-Gene Human Immunity and Metabolic Syndrome 9k. Toxicol In Vitro 24: 85–91.
57. Wolff B, Sanglier JJ, Wang Y (1997) Leptomycin B is an inhibitor of nuclear export: inhibition of nucleo-cytoplasmic translocation of the human immunodeficiency virus type 1 (HIV-1) Rev protein and Rev-dependent mRNA. Chem Biol 4: 139–147.

Journal of Pathology
J Pathol 2011; 224: 420–429
Published online 19 April 2011 in Wiley Online Library
(wileyonlinelibrary.com) DOI: 10.1002/path.2878

ORIGINAL PAPER

Basic helix-loop-helix transcription factor DEC1 negatively regulates cyclin D1

Ujjal K Bhawal,[1,2,10]* Fuyuki Sato,[3] Yuki Arakawa,[4] Katsumi Fujimoto,[5] Takeshi Kawamoto,[5] Keiji Tanimoto,[6] Yumi Ito,[7] Tomonori Sasahira,[2] Takashi Sakurai,[8] Masaru Kobayashi,[9] Isamu Kashima,[8] Hiroshi Kijima,[3] Hiroki Kuniyasu,[2] Yoshimitsu Abiko,[10] Yukio Kato[5] and Sadao Sato[1]

[1] *Research Institute of Occlusion Medicine and Open Research Center, Kanagawa Dental College, Yokosuka, Japan*
[2] *Department of Molecular Pathology, Nara Medical University, Kashihara, Japan*
[3] *Department of Pathology, Hirosaki University Graduate School of Medicine, Hirosaki, Japan*
[4] *Department of Health Science, Division of Oral Health, Kanagawa Dental College, Yokosuka, Japan*
[5] *Department of Dental and Medical Biochemistry, Hiroshima University Graduate School of Biomedical Sciences, Hiroshima, Japan*
[6] *Department of Radiation Medicine, Research Institute for Radiation Biology and Medicine, Hiroshima University, Hiroshima, Japan*
[7] *Department of Comprehensive Dentistry, Kanagawa Dental College, Yokosuka, Japan*
[8] *Division of Radiology, Department of Maxillofacial Diagnostic Science, Kanagawa Dental College, Yokosuka, Japan*
[9] *Department of Oral and Maxillofacial Surgery, Kanagawa Dental College, Yokosuka, Japan*
[10] *Department of Biochemistry and Molecular Biology, Nihon University School of Dentistry at Matsudo, Matsudo, Japan*

**Correspondence to: Ujjal K Bhawal, Department of Biochemistry and Molecuklar Biology, Nihon University School of Dentistry at Matsudo, 2-870-1, Sakaecho-Nishi, Matsudo, Chiba 271-8587, Japan e-mail: bhawal.ujjal.kumar@nihon-u.ac.jp*

Abstract

DEC1 (also known as Stra13/Bhlhb2/Sharp2) and DEC2 (also known as Bhlhb3/Sharp1) are two paralogous basic helix-loop-helix (bHLH) transcriptional regulators which exhibit a robust circadian gene expression pattern in the suprachiasmatic nucleus (SCN) and in peripheral organs. DEC1 has been suggested to play key roles in mammalian cell differentiation, the cell cycle and circadian regulation, hypoxia response, and carcinogenesis. Here we show that DEC1 overexpression exhibits delayed wound healing and reduces cell proliferation, migration, and invasion. DEC1 strongly repressed the promoter activity of cyclin D1. We further identify a possible DEC-response element in the cyclin D1 promoter region, and confirmed the direct binding of DEC1 to that element. Forced expression of DEC1 efficiently repressed the cyclin D1 promoter and expression. Our clinical data provide the first evidence that there is a strong inverse correlation between DEC1 and cyclin D1 expression in oral cancer, and DEC1 expression significantly correlated with clinicopathological parameters. We suggest that radiation-induced DEC1 overexpression and Akt phosphorylation in cancer cells are mediated via PI-3K signalling. Overexpression of DEC1 activates the PI-3K/Akt signalling pathway through reactive oxygen species (ROS).

Keywords: DEC1; cyclin D1; Akt; irradiation; oral cancer

Received 30 September 2010; Revised 12 January 2011; Accepted 10 February 2011

No conflicts of interest were declared.

Introduction

Human differentiated embryonic chondrocyte-expressed genes (DEC), mouse stimulated with retinoic acid (STRA), and rat split and hairy related protein (SHARP) constitute a structurally distinct class of basic helix-loop-helix (bHLH) proteins [1–4]. DEC1 is an important regulator of cellular growth and differentiation [2,5]. The expression level of DEC1 in tumours was positively correlated with tumour grade and the abundance of angiogenic protein vascular endothelial growth factor-D [6–9]. High levels of DEC1 mRNA are also detected in an array of cancer cell lines [10]. DEC1 binds to DNA, causing transcriptional repression [1], and is involved in the regulation of histone deacetylase [11]. DEC1 homologues are involved in cell differentiation [1,3,12], regulation of the circadian system [13,14], and cell cycle regulation [11,15].

Cyclins are essential components of the cell cycle machinery; each binds and activates specific types of cyclin-dependent kinases (CDKs). Cyclin D1 plays an important role in the regulation of G1/S transition [16]. Cyclin D assembles with CDK4/6 in early G1. The accumulation of this complex leads to the activation of the kinases that phosphorylate and inactivate the tumour suppressor retinoblastoma, a necessary step for cell cycle progression through G1 to S phases [17]. Therefore, it has been well established that cyclin D1 plays a crucial role in the progression of the cell cycle

from the G1 to the S phase, and the down-regulation of cyclin D1 will lead to cell cycle arrest at G1 [18,19].

The phosphoinositide-3 kinase (PI-3K)/Akt pathway is also known to play a major role in cell cycle progression during the G1/S transition [20]. Amongst the various substrates of Akt, several of them are involved in cell cycle regulation, including GSK (glycogen synthase kinase)-3β [21]. Akt is capable of phosphorylating GSK-3β at Ser^9 and subsequently inhibiting its kinase activity. Therefore, the Akt–cyclin D1 signalling pathway appears to be crucial in regulating the cell cycle at G1/S transition. Our current efforts have focused on dissecting the role of DEC1 in regulating cyclin D1 in the context of neoplasia.

Materials and methods

Reagents

DEC1 and DEC2 antibodies were kind gifts from Yukio Kato (Hiroshima University, Japan). Cyclin D1 (CC12; Calbiochem, Gibbstown, NJ, USA and SP4; Nichirei Biosciences, Tokyo, Japan) and HIF-1α (BD Biosciences San Diego, CA, USA) antibodies were used. CDK4, CDK6, Akt, GSK-3β, phospho-Akt (Ser473), phospho-GSK-3β (Ser9), GAPDH, and rabbit and mouse IgG antibodies were purchased from Cell Signaling Technology, Inc, Danvers, MA, USA. DEC1 antibody (CW27) was a kind gift from AL Harris (Cancer Research UK Molecular Oncology Laboratory, Oxford, UK). LY294 002 (Calbiochem), catalase (Sigma, Tokyo, Japan) and NE-PER Nuclear and Cytoplasmic Extraction Reagents (Thermo Fisher Scientific Inc, Rockford, IL, USA) were purchased. For all experiments concerning growth, wound healing, and invasion, cells were transfected with expression plasmid or the empty vector for 48 h and transfected cells were then cultured in serum-free media before application.

Cell culture and treatment

All cell lines (HSC-2, HSC-3, and HEK293) were obtained from the Japanese Cancer Research Resources Bank. These cells were cultured in Dulbecco's Modified Eagle's Medium (Sigma Chemical Co, St Louis, MO, USA) supplemented with 10% fetal bovine serum at 37 °C in a humidified atmosphere of 95% air and 5% CO_2. In some experiments, the cells were incubated with LY294 002 at various concentrations for 24 h. In an experiment, cultures were irradiated using an X-ray source at a dose rate of 10 Gy.

Cell viability assay

The cell viability assay was performed using the MTS assay. HEK293 cells were transfected with DEC1 expression plasmid or the empty vector, and cell numbers were counted every 24 h for 2 days in triplicate assays with Cell Titer 96 AQ_{ueous} One Solution Reagent (Promega Corporation, Madison, WI, USA). The absorbance ($OD_{490\ nm}$) was measured using a Microplate reader (iMark™, Bio-rad, Hercules, CA, USA).

Wound healing assay and invasion assay

HEK293 cells were initially seeded uniformly onto 35-mm culture plates with an artificial 'wound' carefully created at 0 h, using a P-1000 pipette tip to scratch on the confluent cell monolayer. Microphotographs were taken at 0 and 12 h. An *in vitro* invasion assay was performed using cell culture inserts (pore size 8 μm) with a thin layer of Matrigel basement membrane matrix (BD Biosciences, Bedford, MA, USA) in 24-well tissue culture plates.

Luciferase reporter assay

To determine the activity of the cyclin D1 promoter in the presence of ectopically overexpressed DEC1, a luciferase assay was performed. The expression plasmid for human DEC1 has been described previously [22]. The cyclin D1 promoter in pCycD1CAT [23] was subcloned into PGL2-basic (Promega Corporation) at the *SmaI* site. In brief, the luciferase reporter plasmid of human cyclin D1 promoter with a potential DEC1-responsive element (DEC1-RE), E-box (CACGTG; −872 to −877), was made by subcloning a 1.9-kb fragment representing nucleotides −1652 to +231 relative to the transcription start site of the cyclin D1 promoter into the vector. 3× Cyclin D1 E-box luc reporter was PCR-amplified from genomic DNA using the following oligonucleotides: 5′-CTAGTatttacacgtgttaatatttacacgtgttaatatttacacgtgttaat-3′ and 5′-TCGAattaacacgtgtaaatattaacacgtgtaaatattaacacgtgtaaatA-3′. This purified fragment was subcloned into the vector pGL3-Basic (Promega Corporation) at the *Nhe*I and *Xho*I sites. The QuikChange Site-Directed Mutagenesis Kit (Stratagene, La Jolla, CA, USA) was used to introduce specific mutations into the E-box binding site within the cyclin D1 promoter. Mutagenetic primers were designed for the E-box binding site with a 6 bp mismatch (in bold): forward, 5′-ctaaattagttcttgcaattta**TCGAAT**ttaatgaaaatgaaagaag-3′; reverse, 5′-cttctttcattttcattaa**ATTCGA**taaattgcaagaactaatttag-3′. The PCR conditions were 18 cycles of 95 °C for 30 s, 55 °C for 60 s, and 68 °C for 10 min. The PGL2-basic vector containing wild-type cyclin D1 promoter was used as template DNA. The sequence of the mutated plasmids was confirmed by DNA sequencing (ABI Prism 3130 Genetic Analyzer, Applied Biosystems, Carlsbad, CA, USA). Transient transfections were performed using FuGENE6™ (Roche, Indianapolis, IN, USA) for HEK293 cells. Luciferase activity was measured with the Dual-luciferase® Reporter Assay System (Promega Corporation) and Turner Designs (Promega Corporation) luminometer. All assays were performed in triplicate and repeated at least three times, and the most representative results are shown.

Chromatin immunoprecipitation (ChIP) assay

The ChIP assay was performed using a kit from Upstate (Charlottesville, VA, USA) as described previously [22]. The primers were designed to amplify the DNA fragment containing the E-box and the sequences of the primers were human cyclin D1-F: 5′-TCCCCGTCCTTGCATGCTAA-3′ and human cyclin D1-R: 5′-AGAATGGGCGCATTTCCAAG-3′. The sequences in the other region (nucleotides −1015 to −1006) of cyclin D1 were human cyclin D1-F: 5′-GGAGATCACTGTTTCTCAGC-3′ and human cyclin D1-R: 5′-TTCTAGCCTGGAGACTCTTC-3′.

Quantitative real-time PCR (QRT-PCR)

Total RNA was isolated using an RNeasy Mini kit (Qiagen, Hilden, Germany) and a TURBO DNA-*free*™ Kit (Applied Biosystems) was used to remove contaminating DNA from RNA preparations. First-strand cDNA was synthesized from 1 μg of total RNA using High Capacity RNA-to-cDNA Master Mix (Applied Biosystems). Real-time PCR was carried out in 96-well plates using the LightCycler® 480 Real-Time PCR System (Roche Applied Science). All reactions were carried out in triplicate. All TaqMan probes (Hs00186419_m1, Hs99999903_m1) were obtained from Applied Biosystems, Japan. Empty luciferase reporter plasmid without reverse transcriptase (RT) was used as a negative control.

Small interfering RNA

The duplexes of each small interfering RNA (siRNA), targeting DEC1 and negative control (non-silencing siRNA or scrambled siRNA) were synthesized by Qiagen, Japan. The siRNAs were transfected into the cells using RNAiMAX (Invitrogen, Carlsbad, CA, USA). The cells were incubated for 48 h and subjected to various analyses.

Western blotting

Cells were lysed in RIPA lysis buffer (Santa Cruz Biotechnology, Santa Cruz, CA, USA). Protein concentration was determined by a BCA Protein Assay Kit (Pierce Biotechnology, Rockford, IL, USA). SDS-polyacrylamide gels were calibrated with molecular weight markers (Bio-Rad), and DEC1, DEC2, cyclin D1, CDK4, CDK6, Akt, GSK-3β, phospho-Akt, phospho-GSK-3β, and GAPDH were used as primary antibodies. Anti-mouse and anti-rabbit secondary antibodies were each used at a dilution of 1 : 2000. Bound antibodies were visualized by chemiluminescence using the ECL Plus Western Blotting Detection System (Amersham, Uppsala, Sweden), and images were analysed by a Luminescent Image Analyzer (LAS-3000; Fuji Film Inc, Japan).

Immunohistochemistry

Initial biopsy specimens were obtained from patients with dysplasias ($n = 30$), *in situ* carcinoma ($n = 15$), and squamous cell carcinoma (SCC) of the tongue and oral floor ($n = 126$), who subsequently underwent treatment with curative intent at Nara Medical University and Tokyo Dental College in Japan. Immunohistochemistry was performed as described previously [8]. The degree of staining was measured as the percentage of positively stained nuclei in 200 tumour cells, as determined by two independent investigators, without knowledge of the specific cases. Cyclin D1 staining was regarded as positive when more than 5% of the tumour cells were stained. DEC1 staining was scored negative, 0–4%; weak, 5–19%; moderate, 20–49%; or strong, >50%. The relationship between either the levels of DEC1 or cyclin D1 and clinicopathological factors was assessed with Fisher's exact test. $p < 0.05$ was considered to be statistically significant.

Immunofluorescent staining

HSC-2 cells were fixed with 4% paraformaldehyde for 15 min before being permeabilized with 0.2% Triton-X-100 in PBS for 5 min. The cells were then washed in PBS twice and treated with protein block (DAKO, Japan) for 30 min before being incubated with DEC1 or cyclin D1 antibodies at 4 °C overnight. The cells were then incubated for 1 h with Alexa Fluor 488-conjugated goat anti-rabbit IgG and counter-stained with ProLong® Gold antifade reagent with DAPI (Molecular Probes, Inc, Eugene, OR, USA) in accordance with the manufacturer's instructions. The cells were visualized using confocal laser scanning microscopy (BZ-8000; Keyence Corporation, Osaka, Japan).

Reactive oxygen species (ROS) detection

DEC1-overexpressing and irradiated HEK293 cells were assayed for intracellular ROS by using an Image-iT™ LIVE green reactive oxygen species detection kit (Molecular Probes), counter-stained with Hoechst 33 342 for nuclei, and imaged under a confocal laser scanning microscope (BZ-8000; Keyence Corporation).

In vivo experiments

Approximately 5×10^6 HSC-2 cells were injected subcutaneously into both sides of the dorso-lateral region of ten female athymic nude mice (BALB/cAJcl-nu/nu; Clea Japan, Tokyo, Japan). Treatment was initiated when the average tumour volume reached 100 mm^3. Mice were exposed to X-ray radiation using a linear accelerator radiation therapy system (HL-1500; Hitachi Medical Corporation, Tokyo, Japan). For radiation fractionation experiments, exposure to 2 Gy was carried out daily for 3 weeks with mice restrained in a thermoplastic shell. The radiation dose was 30 Gy in total. Mice were housed in our approved animal holding facility and treated according to the guidelines of Kanagawa Dental College on Animal Care.

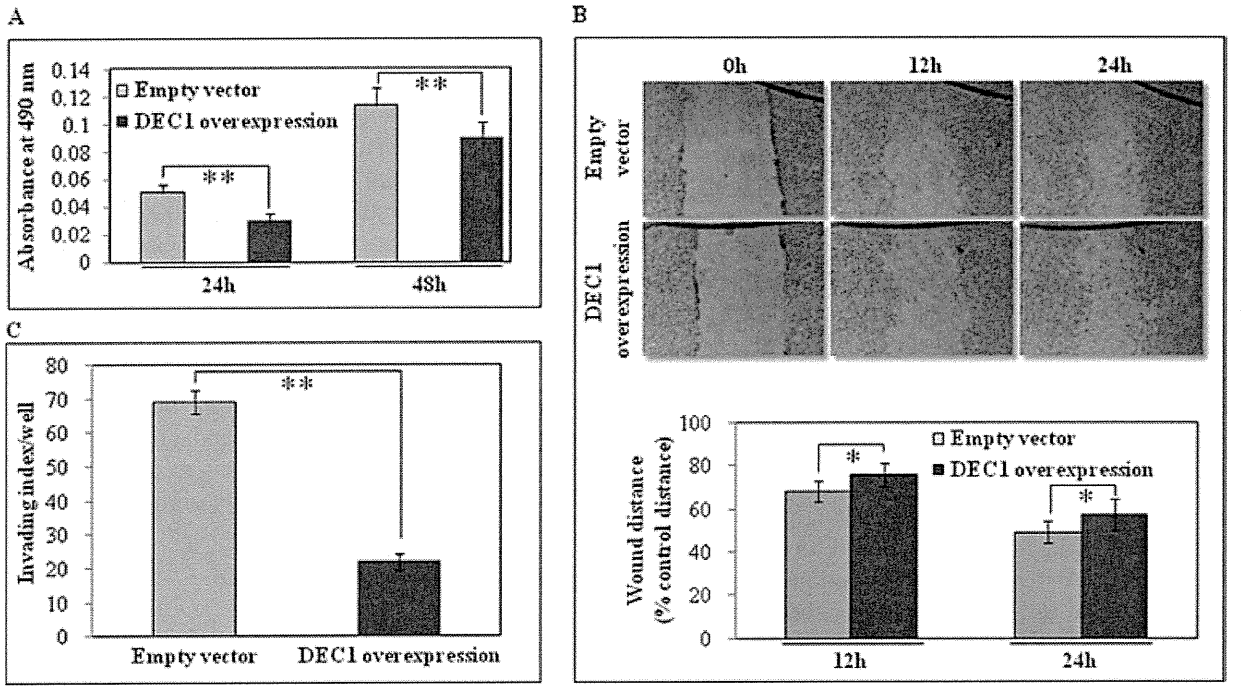

Figure 1. Effects of DEC1 expression on cell proliferation, *in vitro* cell migration, and invasion. (A) The cell viability assay was performed using the MTS assay. HEK293 cells were transfected with DEC1 expression plasmid or the empty vector. Cell numbers were counted every 24 h for 2 days in triplicate assays. (B) For the migration assay, HEK293 cells were transfected with DEC1. Once these monolayers reached confluence, a wound was made with a pipette tip and photographs of the wounded area were taken periodically. (C) For the invasion assay, 48 h post-transfection, 1×10^4 cells each were seeded onto the invasion chamber. After 24 h, the chambers were stained and counted for invaded cells. The experiments were repeated twice in triplicate samples for each. *p* values for comparisons are indicated.

Statistical analysis

Student's two-tailed *t*-test was used to determine the *p* value. $p < 0.05$ was considered to be statistically significant and $p < 0.01$ highly significant.

Results

Effects of DEC1 expression on cell proliferation, *in vitro* cell migration, invasion, and cell cycle distribution

In cells overexpressing DEC1, a diminished cell proliferation rate was observed by the MTS assay. Differences in the cell proliferation rate were significant for those rates obtained between 24 and 48 h (Figure 1A). Next, we tested whether the overexpression of DEC1 would affect wound closure. Figure 1B illustrates how the culture transfected with DEC1 exhibited by the 12th and 24th hour delayed healing in comparison with those transfected with the empty vector. Invasive cells were also significantly reduced in HEK293 cells transfected with DEC1 compared with those transfected with a control vector as determined by invasion assay (Figure 1C).

Identification of cyclin D1 as a direct target of DEC1

The luciferase reporter assay was performed and showed that the luciferase activity of the cyclin D1 promoter reporter was inhibited by DEC1 (Figure 2A). Similar data were observed using the 3× cyclin D1 E-box luc reporter. In contrast, the luciferase activity for the cyclin D1 promoter with a mutated E-box was inert. We confirmed the increased levels of DEC1 mRNA in the transfected cells by quantitative real-time RT-PCR (Figure 2B). Empty luciferase reporter plasmid without RT was used as a negative control. Next, we examined whether DEC1 can bind to the E-box in the cyclin D1 gene *in vivo*. DEC1 bound to the E-box of the cyclin D1 gene (Figure 2C). These data indicate that cyclin D1 is likely to be a direct target gene of DEC1. Western blot analysis of cell extracts showed that the levels of cyclin D1, CDK4, and CDK6 protein were reduced in DEC1-overexpressing cells (Figure 2D). We also found Akt phosphorylation at Ser^{473} and GSK-3β phosphorylation at Ser^{9} in DEC1-overexpressing cells (Figure 2D).

In order to demonstrate specific binding of endogenous DEC1 to the cyclin D1 promoter, we performed a ChIP assay using anti-DEC1 antibody with/without siRNA for DEC1 in HSC-3 cells. The results showed that anti-DEC1 antibody specifically precipitated the cyclin D1 promoter region and siRNA for DEC1 inhibited it (Figure 2E). We then examined if knockdown of DEC1 would reverse the repression of cyclin D1. Unexpectedly, siRNA-mediated knockdown of DEC1 also resulted in a decrease of the cyclin D1 protein level (Figure 2E), as seen in overexpression of DEC1. Furthermore, siRNA-mediated knockdown of DEC2 also decreased the cyclin D1 level. Interestingly, DEC1

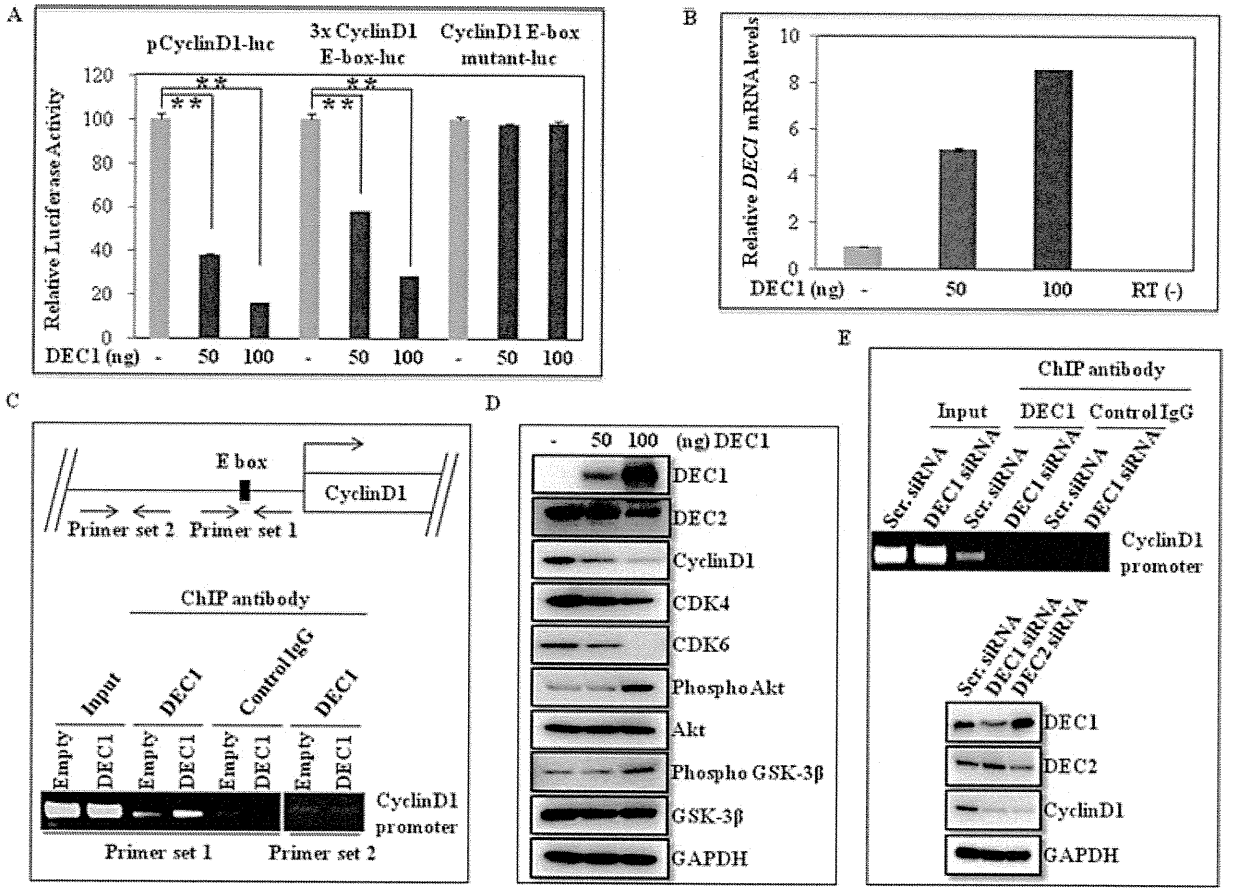

Figure 2. DEC1 binds to and transactivates the cyclin D1 promoter. (A) Luciferase reporter assay. HEK293 cells were transfected with cyclin D1-luc (firefly), *Renilla* luciferase, and increasing amounts of DEC1 (left). 3× Cyclin D1 E-box-luc reporter was generated and was introduced into HEK293 cells with or without DEC1 (middle) and the effect of E-box mutation on the activity of the cyclin D1 promoter was noted (right). Following 48 h culture, luciferase activity was measured and normalized to *Renilla* luciferase activity. Columns, mean of three independent experiments carried out in triplicate; bars, SE. $*p < 0.05$. (B) DEC1 mRNA was analysed in transfected HEK293 cells by the quantitative real-time PCR method. Empty luciferase reporter plasmid without reverse transcriptase (RT) was used as a negative control. Relative mRNA levels were calculated as the ratio to that of ACTB, and each bar represents the mean ± SD for at least three independent experiments. (C) ChIP assay was carried out by overexpressing DEC1 in HEK293 cells. Twenty-four hours post-transfection, cells were collected for ChIP. PCR was performed with the eluted DNA fragments. Anti-rabbit IgG was used as an immunoprecipitation control. Another region (nucleotides −1015 to −1006) of the cyclin D1 promoter was also used. (D) Total cell lysates were prepared from HEK293 cells transiently transfected with DEC1 and equivalent amounts of protein were resolved by SDS-PAGE, blotted, and probed with the indicated antibodies. (E) ChIP assay was performed with/without siRNA for DEC1 in HSC-3 cells (top). The effect of DEC1 knockdown on cyclin D1 expression in HSC-3 cells was shown (bottom).

knockdown increased the DEC2 protein level and vice versa (Figure 2E).

The levels of DEC1 correlate with the level of cyclin D1, tumour stage, and clinical stage in SCC tumours

Representative examples of immunohistochemical staining are shown in Figure 3. DEC1 expression in normal human oral tissues was present predominantly in the granular and spinous layers of epithelial cells, but parabasal cell staining was occasionally present. In dysplasias, DEC1 expression was present predominantly in the parabasal layer of epithelial cells. In oral carcinomas, expression of DEC1 was nuclear and immunopositivity was homogeneous throughout the tumour. Table 1 indicates that of the 126 tumours, 34 were positive for DEC1 (27%). Sixty of 126 tumours were positive for cyclin D1 (48%). Only five cases were positive for both DEC1 and cyclin D1. Our clinical data provide the first evidence that there is a strong inverse correlation between DEC1 and cyclin D1 expression in SCC ($p \leq 0.0001$; Table 1). DEC1 expression also correlated significantly with tumor stage ($p = 0.0002$) and clinical stage ($p = 0.0006$), whereas cyclin D1 did not correlate significantly with any of these parameters (Table 2). The positive expression rate of DEC1 protein in the moderately or poorly differentiated tumour tissues was 12%, which was lower than that in well-differentiated tumour tissues ($p = 0.001$).

Up-regulation of DEC1 by DNA damage

DEC1 expression was induced in irradiated HSC-2 cells, while cyclin D1 expression was decreased (Figures 4A and 4B). As expected, phosphorylation of Akt was up-regulated by irradiation (Figure 4B). The

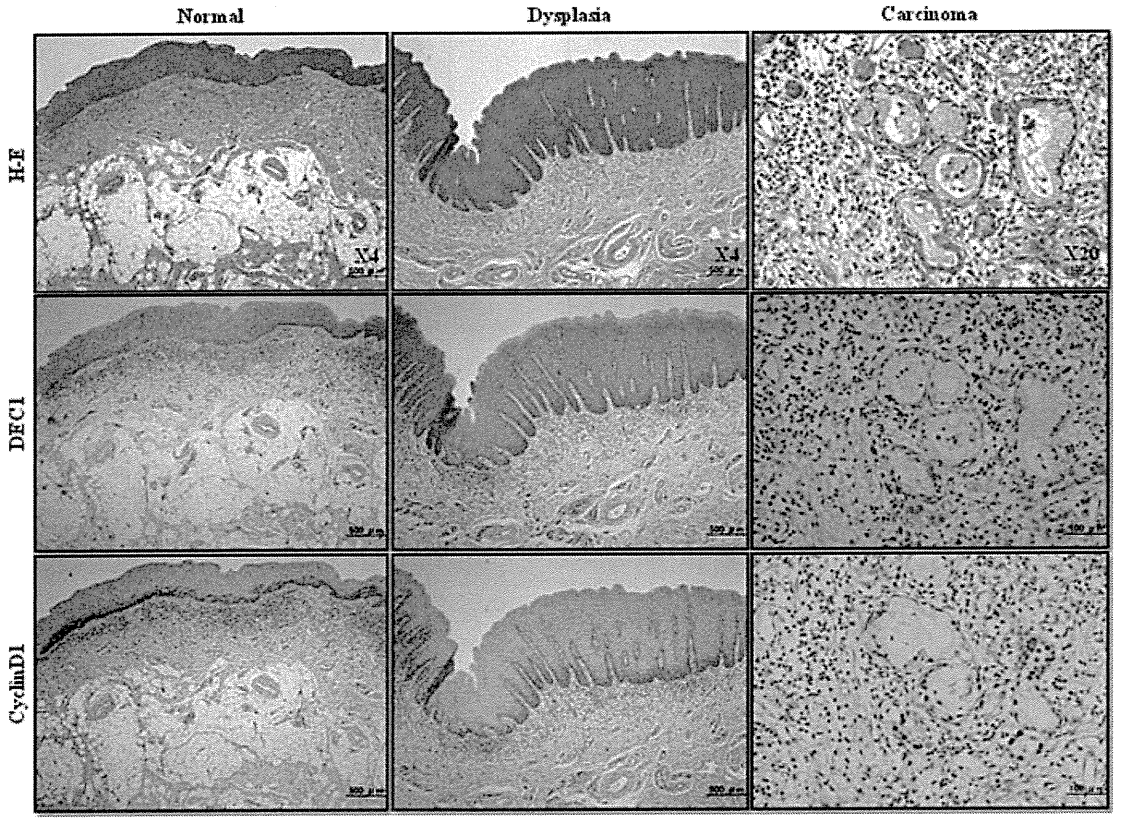

Figure 3. The levels of DEC1 correlate with the level of cyclin D1, tumour stage, and clinical stage in SCC. Immunostaining of DEC1 and cyclin D1 was performed on 4 μm thick sections of formalin-fixed and paraffin-embedded tumour specimens using the rabbit polyclonal antiserum to the pDEC1 C-terminus and rabbit monoclonal cyclin D1 antibody. Sections were deparaffinized and immunoreactivity was detected using the Dako Envision Kit.

Table 1. Correlation between DEC1 and cyclin D1 in oral cancer

	Cyclin D1 staining			
DEC1 staining	Negative $n = 66$	Positive $n = 60$	Total	p
Negative, $n = 92$	37 (29%)	55 (44%)	92 (73%)	
Positive, $n = 34$	29 (23%)	5 (4%)	34 (27%)	< 0.0001*
Total	66 (52%)	60 (48%)	126 (100%)	

*Fisher's exact test.

nuclear level of DEC1 was substantially increased at 24 h after irradiation (Figure 4C). We also examined if knockdown of DEC1 would affect the phosphorylation of Akt in HSC-2 cells. We found that siRNA against DEC1 decreases the expression of Akt phosphorylation (Figure 4D). Pretreatment with LY294 002 abrogated the irradiation-induced Akt phosphorylation and DEC1 expression in HSC-2 cells (Figure 4E). To determine ROS generation by DEC1 overexpression and irradiation, we examined intracellular ROS levels in DEC1-overexpressing and irradiated HEK293 cells. We showed that DEC1 overexpression and irradiation induced ROS generation. Preincubation of cells with catalase reduced the fluorescent intensities (Figure 5A). The tumours of mice treated with irradiation showed stronger DEC1 staining than those of mice in the control group (Figure 5B). Compared with the controls, mice with HSC-2 tumour treated with irradiation had weaker cyclin D1 staining.

Discussion

DEC1 is believed to be involved in the control of proliferation and/or differentiation of various types of cells [3]. Because some transcription factors are involved in the regulation of cell proliferation, we analysed whether DEC1 was able to affect the transcription of cyclin D1, a key regulator of the cell cycle. Our results indicated that DEC1 repressed the transcription of the cyclin D1 gene. This repression seemed to be physiologically relevant, because cells overexpressing DEC1 exhibited a diminished cell proliferation and invasion rate, as determined through MTS assay, *in vitro* wound healing assay, and *in vitro* invasion assay (Figures 1B–1D). In a previous study, NIH3T3 cells transfected with DEC1 exhibited a reduction in colony-forming numbers compared with cells transfected with an empty vector [11]. Transfection with DEC1 decreases cell proliferation, and the decrease is proportionally correlated with the levels of DEC1 [24].

Table 2. Correlations between DEC1 or cyclin D1 and clinicopathological parameters in oral cancer

	No	DEC1 expression	p	Cyclin D1 expression	p
T stage					
I and II	78	30 (38%)	0.0002*	39 (50%)	0.58
III and IV	48	4 (8%)		21 (44%)	
Clinical stage					
I and II	64	26 (41%)	0.0006*	27 (42%)	0.28
III and IV	62	8 (13%)		33 (53%)	
Well differentiated	75	28 (37%)	0.0019*	40 (53%)	< 0.0001
Moderately or poorly differentiated	51	6 (12%)		47 (92%)	

*Fisher's exact test.

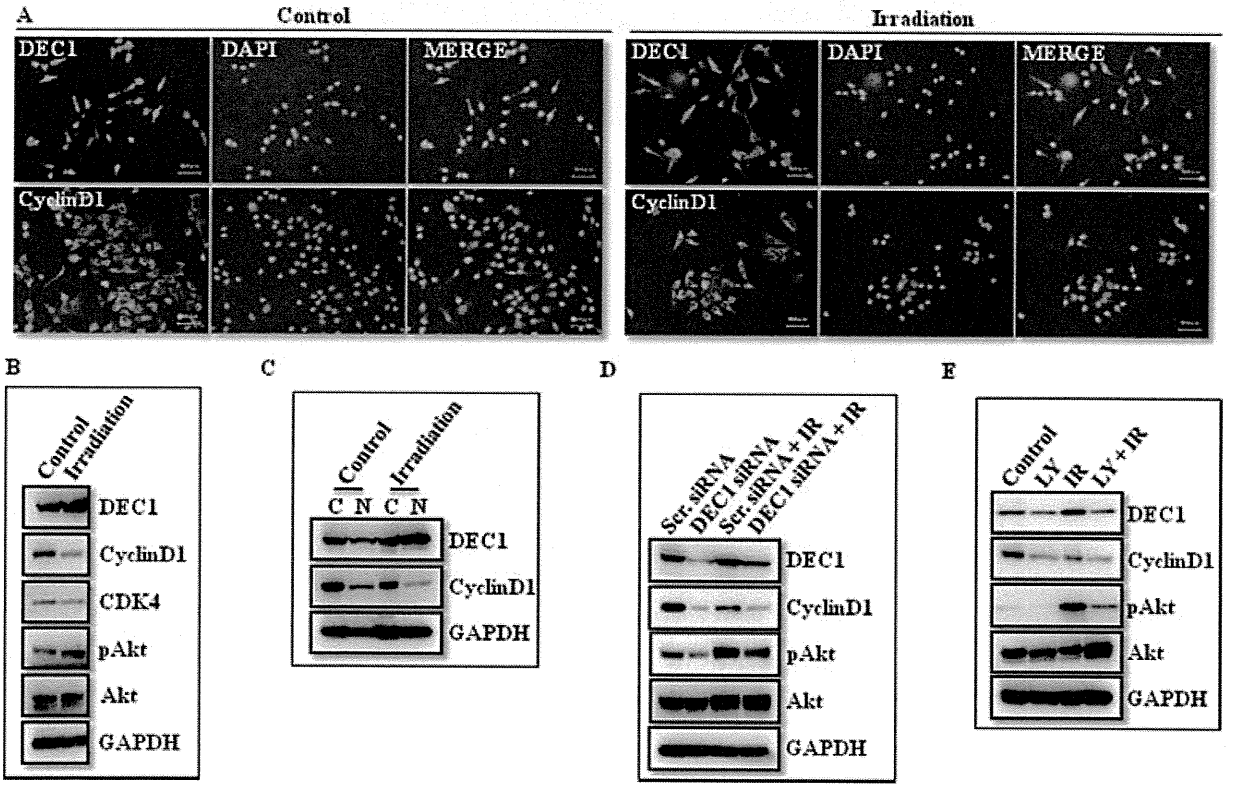

Figure 4. Radiation-induced DEC1 overexpression and Akt phosphorylation in cancer cells is mediated via PI-3K signalling. (A) HSC-2 cells were seeded in a four-chamber slide glass and probed with anti-DEC1 or anti-cyclin D1 antibodies at 4 °C overnight. The cells were then incubated for 1 h with goat anti-rabbit IgG antibody conjugated to Alexa Fluor 488, and counter-stained with ProLong® Gold antifade reagent with DAPI. (B) Immunoblotting analysis was performed with the indicated antibodies using whole cell extract prepared from HSC-2 cells treated with 10 Gy radiation for a 24-h interval. (C) Nuclear and cytoplasmic protein fractions were isolated from cultured HSC-2 cells treated with 10 Gy radiation and western blot analysis was performed with the indicated antibodies. (D) HSC-2 cells were transfected with DEC1 siRNA along with scramble siRNA as a control. The cells were incubated for 48 h and then treated with irradiation for another 24 h and subjected to western blot analysis with the indicated antibodies. (E) HSC-2 cells were pretreated with LY294002 for 1 h, followed by 10 Gy radiation for 24 h. Whole cell lysates were prepared and aliquots were subjected to immunoblot assays using the indicated antibodies.

DNA binding is probably the primary mechanism responsible for DEC1-mediated repression of the expression of cyclin D1. Our results suggest that the E-box may be a critical target for cyclin D1 transcription, although several other regulatory elements such as binding sites for Sp1, Ets, CREB, and E2F have also been identified in the promoter region of the cyclin D1 gene [25]. Transfection of siRNA against DEC1 failed to reverse the repression of cyclin D1, since knockdown of DEC1 increased the expression of DEC2 and vice versa (Figure 2E). Indeed, forced expression of DEC1 resulted in repression of the activity of a DEC2 promoter reporter [26]. Li *et al* had shown that DEC1 represses the expression of DEC2 through binding to the E-box in the DEC2 promoter [27]. We previously reported similar functions that DEC1 knockdown induces DEC2 expression, and both of them regulate the MLH1 promoter [28]. DEC2 also binds to the E-box of various genes and may suppress the expression of cyclin D1 by binding to the E-box elements of the promoter. Taken together, these results suggest that both DEC1 and DEC2 regulate cyclin D1 expression.

Statistical analysis showed no differences in the expression of cyclin D1 between low- and high-grade oral cancers. A tendency of higher expression towards moderately or poorly differentiated oral cancer was

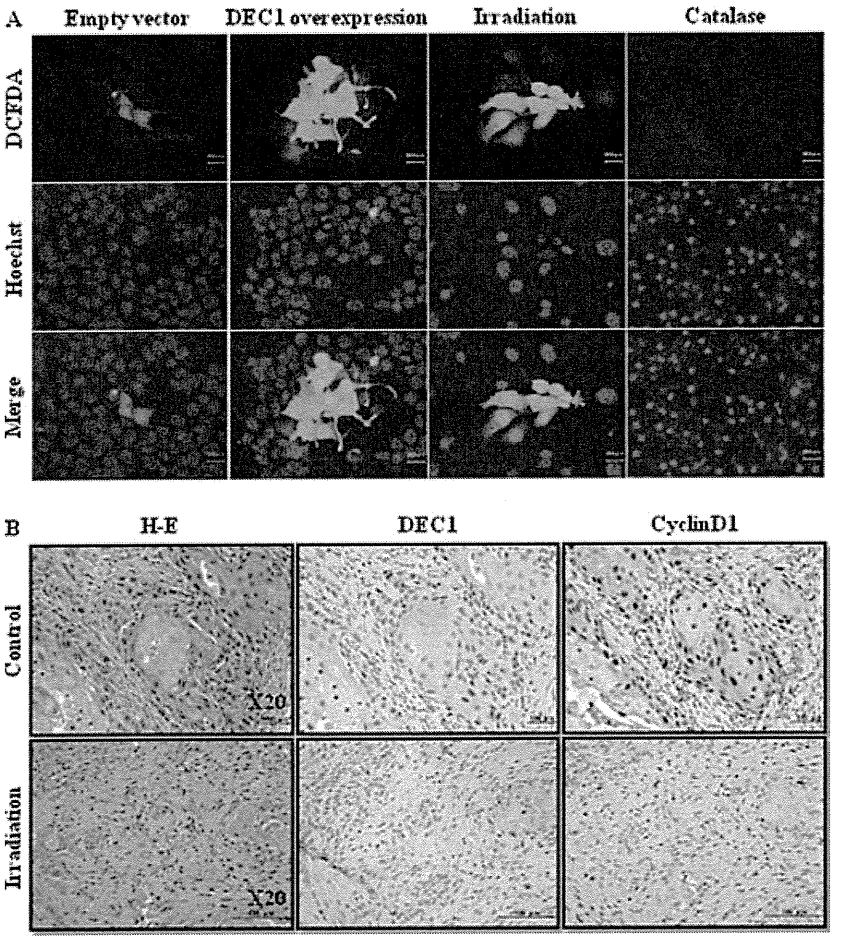

Figure 5. DEC1 overexpression increases ROS and up-regulation of DEC1 upon DNA damage in a mouse xenograft. (A) To visualize intracellular ROS levels, empty vector or DEC1-overexpressing and irradiated HEK293 cells were assayed for intracellular ROS by using the Image-iT™ LIVE green reactive oxygen species detection kit. Intracellular ROS were visualized using a confocal microscope. (B) Mice were exposed to X-ray radiation using a linear accelerator radiation therapy system. The radiation dose was 30 Gy in total. Twenty-five days later, the mice were sacrificed and their tumours were excised and processed for histology. Anti-DEC1 and anti-cyclin D1 antibodies were used for immunohistochemical analysis.

noted. The higher expression of cyclin D1 in tumours might be explained by the fact that alterations in cyclin D1 are related to an intense proliferative activity and invasiveness capacity of the lesions. In contrast, the absence of cyclin D1 can be related to the deregulation of other proteins in the cycle.

The inverse association of DEC1 with proliferation is probably related to its role in cellular differentiation and apoptosis resistance [1,3,10]. The worse the cancer cell differentiation, the lower was the DEC1 protein expression (Table 2). This is exactly what we expected, as DEC1 plays a role in cellular differentiation by stabilizing the cytoskeleton through binding to actin [29], or DEC1 is a transcriptional repressor whose expression is associated with induction of growth arrest and terminal differentiation [30]. DEC1 is also a hypoxia-regulated gene, and the marked induction of this differentiation factor by hypoxia within tumours suggests that it may be predominantly regulated by hypoxia and that hypoxia may have a role in differentiation. We did not demonstrate a significant association between DEC1-positive tumours and relapse-free or overall survival which has been reported for hypoxic node-negative and node-positive breast tumours [31,32], although there was a trend of increasingly worse prognosis in SCC patients showing down-regulation of DEC1 (data not shown). We suggest that DEC1 is a critical connecting node for cell proliferation.

Growing evidence suggests that ROS act as second messengers in intracellular signalling cascades that induce and maintain the oncogenic phenotype of tumoural cells. ROS have been described to induce proliferation, survival, and cellular migration [33–35]. ROS can directly modify signalling proteins through nitrosylation, carbonylation, glutathionylation, and the formation of disulphide bonds [36]. Since ROS have been reported as potent activators of the PI-3K/Akt pathway, we measured ROS generation in response to DEC1 overexpression in HEK293 cells. The level of ROS in living cells was assessed using the fluorescent probe DCFDA. DEC1-overexpressing cells showed a clear increase of ROS with respect to their counterparts. Irradiation also increased cellular ROS (Figure 5A). The observed increase in cellular ROS was inhibited by treatment with catalase. These results suggest that the

generation of ROS acts as a mediator of DEC1-induced survival through PI-3K/Akt signalling.

In summary, we have shown that DEC1 inhibits the transcription of cyclin D1, and this inhibition is associated with the E-box in the cyclin D1 promoter. The interaction of DEC1 with the E-box is important for understanding the role played by transcription factors in the regulation of cell proliferation and tumourigenesis. We have also demonstrated that DEC1 is an effector of the Akt-dependent DNA damage response pathway. Our data provide insight into the molecular mechanisms of oral cancer and reveal DEC1 as a novel molecular target for cancer therapeutic strategies.

Acknowledgment

We thank Professor Y Tanaka (Tokyo Dental College), Professor A Hara (Gifu University), Dr K Yamamoto (Nara Medical University), Dr T Ikoma, and Dr C Taguchi (Kanagawa Dental College) for their helpful contributions to this work. This work was supported by Grants-in-Aid (21791801; UK Bhawal) for Young Scientists from the Ministry of Education, Culture, Sports, Science and Technology of Japan.

Author contribution statement

UKB was involved in conception and design; acquisition, analysis, and interpretation of data; and drafting the article. FS made a substantial contribution to conception and design, data acquisition, and revision of the article. YuA and TaS were involved in acquisition, analysis, and interpretation of data, and revising the article. KF and KT made a substantial contribution to conception and design, interpretation of data, and revising the article. TK, YI, ToS, MK, IK, HKi, YoA, YK, and SS were involved in data interpretation and revising the article. HKu made a substantial contribution to conception and design, and revising the article.

References

1. Boudjelal M, Taneja R, Matsubara S, *et al*. Overexpression of Stra13, a novel retinoic acid-inducible gene of the basic helix-loop-helix family, inhibits mesodermal and promotes neuronal differentiation of P19 cells. *Genes Dev* 1997; **11**: 2052–2065.
2. Rossner MJ, Dorr J, Gass P, *et al*. SHARPs: mammalian enhancer-of-split- and hairy-related proteins coupled to neuronal stimulation. *Mol Cell Neurosci* 1997; **9**: 460–475.
3. Shen M, Kawamoto T, Yan W, *et al*. Molecular characterization of the novel basic helix-loop-helix protein DEC1 expressed in differentiated human embryo chondrocytes. *Biochem Biophys Res Commun* 1997; **236**: 294–298.
4. Fujimoto K, Shen M, Noshiro M, *et al*. Molecular cloning and characterization of DEC2, a new member of basic helix-loop-helix proteins. *Biochem Biophys Res Commun* 2001; **280**: 164–171.
5. Zhong TP, Rosenberg M, Mohideen MA, *et al*. Gridlock, an HLH gene required for assembly of the aorta in zebrafish. *Science* 2000; **287**: 1820–1824.
6. Giatromanolaki A, Koukourakis MI, Sivridis E, *et al*. DEC1 (STRA13) protein expression relates to hypoxia-inducible factor 1-alpha and carbonic anhydrase-9 overexpression in non-small cell lung cancer. *J Pathol* 2003; **200**: 222–228.
7. Chakrabarti J, Turley H, Campo L, *et al*. The transcription factor DEC1 (stra13, SHARP2) is associated with the hypoxic response and high tumour grade in human breast cancers. *Br J Cancer* 2004; **91**: 954–958.
8. Turley H, Wykoff CC, Troup S, *et al*. The hypoxia-regulated transcription factor DEC1 (Stra13, SHARP-2) and its expression in human tissues and tumours. *J Pathol* 2004; **203**: 808–813.
9. Currie MJ, Hanrahan V, Gunningham SP, *et al*. Expression of vascular endothelial growth factor D is associated with hypoxia inducible factor (HIF-1alpha) and the HIF-1alpha target gene DEC1, but not lymph node metastasis in primary human breast carcinomas. *J Clin Pathol* 2004; **57**: 829–834.
10. Ivanova AV, Ivanova SV, Danilkovitch-Miagkova A, *et al*. Regulation of STRA13 by the von Hippel–Lindau tumor suppressor protein, hypoxia, and UBC9/ubiquitin proteasome degradation pathway. *J Biol Chem* 2001; **276**: 15306–15315.
11. Sun H, Taneja R. Stra13 expression is associated with growth arrest and represses transcription through histone deacetylase (HDAC)-dependent and HDAC-independent mechanisms. *Proc Natl Acad Sci U S A* 2000; **97**: 4058–4063.
12. Shen M, Yoshida E, Yan W, *et al*. Basic helix-loop-helix protein DEC1 promotes chondrocyte differentiation at the early and terminal stages. *J Biol Chem* 2002; **277**: 50112–50120.
13. Honma S, Kawamoto T, Takagi Y, *et al*. Dec1 and Dec2 are regulators of the mammalian molecular clock. *Nature* 2002; **419**: 841–844.
14. Grechez-Cassiau A, Panda S, Lacoche S, *et al*. The transcriptional repressor STRA13 regulates a subset of peripheral circadian outputs. *J Biol Chem* 2004; **279**: 1141–1150.
15. Sun H, Lu B, Li RQ, *et al*. Defective T cell activation and autoimmune disorder in Stra13-deficient mice. *Nature Immunol* 2001; **2**: 1040–1047.
16. Weinberg RA. The retinoblastoma protein and cell cycle control. *Cell* 1995; **81**: 323–330.
17. Harbour JW, Dean DC. The Rb/E2F pathway: expanding roles and emerging paradigms. *Genes Dev* 2000; **14**: 2393–2409.
18. Malumbres M, Barbacid M. Cell cycle, CDKs and cancer: a changing paradigm. *Nature Rev Cancer* 2009; **9**: 153–166.
19. Blain SW. Switching cyclin D–Cdk4 kinase activity on and off. *Cell Cycle* 2008; **7**: 892–898.
20. Liang J, Slingerland JM. Multiple roles of the PI3K/PKB (Akt) pathway in cell cycle progression. *Cell Cycle* 2003; **2**: 339–345.
21. Blume-Jensen P, Hunter T. Oncogenic kinase signaling. *Nature* 2001; **411**: 355–365.
22. Sato F, Bhawal UK, Kawamoto T, *et al*. Basic-helix-loop-helix (bHLH) transcription factor DEC2 negatively regulates vascular endothelial growth factor expression. *Genes Cells* 2008; **13**: 131–144.
23. Ohtani K, DeGregori J, Nevins JR. Regulation of the cyclin E gene by transcription factor E2F1. *Proc Natl Acad Sci U S A* 1995; **92**: 12146–12150.
24. Li Y, Zhang H, Xie M, *et al*. Abundant expression of Dec1/stra13/sharp2 in colon carcinoma: its antagonizing role in serum deprivation-induced apoptosis and selective inhibition of procaspase activation. *Biochem J* 2002; **367**: 413–422.
25. Matsumura I, Kitamura T, Wakao H, *et al*. Transcriptional regulation of the cyclin D1 promoter by STAT5: its involvement in cytokine-dependent growth of hematopoietic cells. *EMBO J* 1999; **18**: 1367–1377.
26. Azmi S, Sun H, Ozog A, *et al*. mSharp-1/DEC2, a basic helix-loop-helix protein functions as a transcriptional repressor of E